HHS Public Access

Author manuscript

Cell Rep. Author manuscript; available in PMC 2024 July 10.

Published in final edited form as:

Cell Rep. 2024 June 25; 43(6): 114278. doi:10.1016/j.celrep.2024.114278.

Hippocampal astrocytes induce sex-dimorphic effects on memory

Samantha M. Meadows[1,2,3], **Fernando Palaguachi**[1,2], **Minwoo Wendy Jang**[1,2], **Avital Licht-Murava**[1,2], **Daniel Barnett**[1,2,3], **Till S. Zimmer**[1,2], **Constance Zhou**[1,2,4], **Samantha R. McDonough**[1,2,3], **Adam L. Orr**[1,2,3], **Anna G. Orr**[1,2,3,4,5,*]

[1]Helen and Robert Appel Alzheimer's Disease Research Institute, Weill Cornell Medicine, New York, NY 10021, USA

[2]Feil Family Brain and Mind Research Institute, Weill Cornell Medicine, New York, NY 10021, USA

[3]Neuroscience Graduate Program, Weill Cornell Medicine, New York, NY 10021, USA

[4]Weill Cornell/Rockefeller/Sloan Kettering Tri-Institutional MD-PhD Program, New York, NY 10021, USA

[5]Lead contact

SUMMARY

Astrocytic receptors influence cognitive function and can promote behavioral deficits in disease. These effects may vary based on variables such as biological sex, but it is not known if the effects of astrocytic receptors are dependent on sex. We leveraged *in vivo* gene editing and chemogenetics to examine the roles of astrocytic receptors in spatial memory and other processes. We show that reductions in metabotropic glutamate receptor 3 (mGluR3), the main astrocytic glutamate receptor in adults, impair memory in females but enhance memory in males. Similarly, increases in astrocytic mGluR3 levels have sex-dependent effects and enhance memory in females. mGluR3 manipulations also alter spatial search strategies during recall in a sex-specific manner. In addition, acute chemogenetic stimulation of $G_{i/o}$-coupled or G_s-coupled receptors in hippocampal astrocytes induces bidirectional and sex-dimorphic effects on memory. Thus, astrocytes are sex-dependent modulators of cognitive function and may promote sex differences in aging and disease.

In brief

*Correspondence: ago2002@med.cornell.edu.

AUTHOR CONTRIBUTIONS

Conceptualization, S.M.M., A.L.M., A.L.O., and A.G.O.; methodology, S.M.M., A.L.M., A.L.O., and A.G.O.; investigation, all co-authors; formal analysis, S.M.M., M.W.J., T.S.Z., C.Z., and A.G.O.; visualization, S.M.M., M.W.J., and A.G.O.; funding, S.M.M. and A.G.O.; supervision, A.L.O. and A.G.O.; writing – original draft, S.M.M. and A.G.O.; writing – review & editing, all co-authors.

DECLARATION OF INTERESTS

The authors declare no competing interests.

SUPPLEMENTAL INFORMATION

Supplemental information can be found online at https://doi.org/10.1016/j.celrep.2024.114278.

Meadows et al. identify sex-dependent effects of glial receptors on neurocognitive function. Changes in mGluR3 levels or activation of $G_{i/o}$-coupled or G_s-coupled receptors in adult hippocampal astrocytes had divergent effects on memory across sexes. These results suggest that astrocytic receptors promote sex differences in behavior.

Graphical Abstract

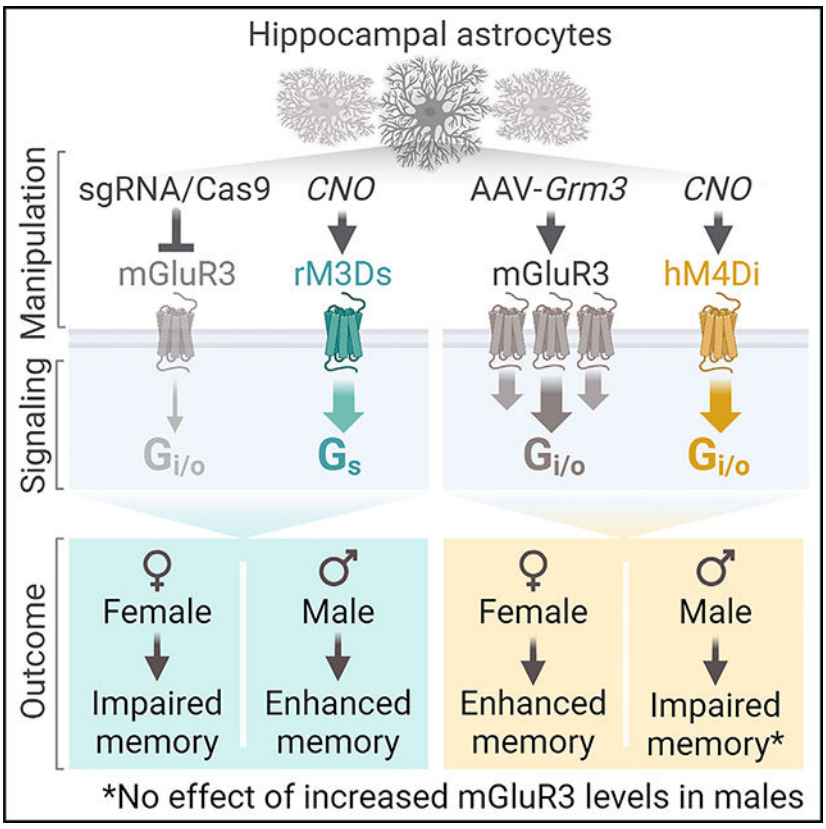

INTRODUCTION

Astrocytes are abundant non-neuronal cells that regulate many aspects of neural function, including cognitive processes and behavior, partly through close interactions with neurons.[1,2] Astrocytic G-protein-coupled receptors (GPCRs) mediate astrocytic-neuronal interactions and are increasingly recognized as influencing memory and other cognitive functions.[3–12] Metabotropic glutamate receptor 3 (mGluR3) is a $G_{i/o}$-coupled receptor enriched in astrocytes throughout the hippocampus, neocortex, striatum, and other brain regions.[13–16] Although astrocytic mGluR3 is highly expressed in astrocytes and considered a primary astrocytic sensor of glutamate, its roles in adult brain function are not defined.[17,18]

The levels of mGluR3 are altered in diverse pathological conditions.[19–25] The gene transcript encoding mGluR3 (*GRM3*) is among the top most reduced astrocytic genes in Alzheimer's disease, and single-nucleotide polymorphisms in *GRM3* are associated with cognitive dysfunction and neuropsychiatric disorders, including schizophrenia and bipolar

disorder.[19,20,23,26–28] Despite its associations with neurocognitive and behavioral disorders, and mGluR3-targeting therapeutics in development,[29–31] the effects of altered astrocytic mGluR3 function on cognitive and behavioral changes remain unknown. Astrocytic receptors are implicated in numerous behavioral disorders, and these disorders vary by sex in their prevalence, risk factors, progression, and response to therapeutics. However, the effects of astrocyte receptors, including mGluR3, across sexes have not been assessed.

Here, we explored whether astrocytic mGluR3 regulates hippocampus-dependent learning and memory and other behavioral functions. We carried out CRISPR-Cas9-based gene editing or induced adeno-associated virus (AAV)-mediated mGluR3 expression selectively in hippocampal astrocytes *in vivo*, in conjunction with in-depth behavioral analyses. We also performed complementary chemogenetic manipulations to assess the cognitive effects of astrocytic receptor activation *in vivo*.

RESULTS

Reductions in astrocytic mGluR3 induce sex-specific effects on memory

We first tested whether perturbations in astrocytic mGluR3 affect hippocampus-dependent cognitive functions, including learning and memory. We used astrocyte-targeted CRISPR-Cas9-based gene editing (Figure 1A). We generated *Aldh1l1*-CreER^{T2}:LSL-Cas9-EGFP mice (hereafter, *Aldh1l1*-Cas9) that enabled astrocyte-selective and tamoxifen (TAM)-inducible Cas9-EGFP expression in approximately 20% of hippocampal astrocytes in adult males and females (Figures 1B, 1C, and S1A–S1C). To selectively disrupt the gene encoding mGluR3 (*Grm3*), mice received intrahippocampal injections of PHP.eB AAV vectors[32,33] encoding *Grm3*-targeting sgRNAs 1 week prior to TAM. This approach resulted in astrocyte-selective, partial loss of mGluR3, consistent with the mosaic pattern of Cas9-EGFP expression in hippocampal astrocytes (Figures S1B–S1D). mGluR3 was detected throughout the hippocampus but was enriched in the molecular layer of the dentate gyrus (Figures 1B and S1A), consistent with recent transcriptomic analyses.[16,34] In *Aldh1l1*-Cas9 mice receiving *Grm3*-targeting single guide RNAs (sgRNAs), mGluR3 immunoreactivity was reduced by 45%, and *Grm3* mRNA levels were reduced by 25% (Figures 1D, 1E, and S1E), and at 5–7 months of age, baseline *Grm3* mRNA and mGluR3 protein levels were similar between sexes (Figure S1F). There were no detectable sgRNA-induced changes in other types of mGluRs (Figure S1G), including mGluR2, which has close sequence homology with mGluR3. Thus, knockdown was selective and without alterations in other related glutamate receptors, in contrast to the changes reported in constitutive global knockout mice.[35] mGluR3 remained intact in other brain regions (Figures S1H and S1I).

We used the Morris water maze to assess spatial learning during hidden platform training and spatial memory in recent and remote probe trials (1 and 9 days after training, respectively). We coupled this paradigm with automated analyses to enable unbiased and multifaceted assessments of (1) learning over time, (2) preferences for target zones relative to other areas of the maze (i.e., target quadrant and platform location) (Figure 1F), (3) specific types of search strategies, (4) accuracy of starting trajectories to approach the target, and (5) motor abilities.[36–40] The hippocampus also facilitates novelty processing and anxiety,[41,42] which were assessed using the elevated plus maze (EPM)[43,44] (Figure S1J).

At 5–7 months of age, knockdown of astrocytic mGluR3 did not affect learning or swimming abilities (Figures 1G and S2A–S2E). However, females with mGluR3 knockdown had impaired memory recall in probe trials, reflected by the lack of target quadrant and target platform preferences vs. other locations at 1 and 9 days after training (Figures 1H–1J). In contrast to the deficits in females, male mice with mGluR3 knockdown had enhanced target preferences, especially at 9 days after training, when the control males no longer had significant target preferences (Figures 1J and S2F). We further evaluated the effects of sex by converting the raw measurements into index values, in which scores of 0.5 and below reflected a lack of preference for target location (individual target values divided by the sum of target and mean of other/nontarget values) (Figures 1H–1J). We also compared the relative changes in index values across sexes in response to knockdown (fold change), where values below 1.0 reflected impairments and above 1.0 reflected improvements as compared to same-sex controls. Average index values were similar among sexes in control groups but different in sgRNA groups (Figures 1H–1J), indicative of differential effects of mGluR3 reduction in males vs. females. Similarly, the relative changes in index values were different between sexes (Figures 1H–1J).

In the EPM, another task that involves hippocampal function, astrocytic mGluR3 knockdown reduced novelty-related exploration in females but increased this exploration in males (Figure S2G), consistent with previous findings in male mice with global mGluR3 gene ablation.[45] Anxiety-like behavior was not significantly affected in males or females (Figure S2H). Thus, mGluR3 knockdown caused divergent, sex-specific effects on hippocampus-dependent behaviors in different behavioral test modalities.

Increases in astrocytic mGluR3 enhance memory in females but not males

We next examined if the sex-dependent effects on memory were specific to the loss of mGluR3 or if other types of mGluR3 alterations also induce sex-specific changes in behavior. We therefore tested if enhancing mGluR3 levels in hippocampal astrocytes is sufficient to alter cognition in a sex-dependent manner. These experiments used middle-aged mice (12–14 months of age), which have potentially earlier onset of spatial memory deficits in females as compared to males in certain behavioral paradigms. Specifically, female mice develop some memory deficits in the Morris water maze by 12–14 months of age, whereas deficits are evident at later ages in males (18 months or older).[46] Thus, we asked whether increases in astrocytic mGluR3 are sufficient to enhance performance in middle-aged females and if memory in males is also differentially affected.

We delivered AAV vectors encoding Cre-dependent, hemagglutinin (HA)-tagged mGluR3 under the control of astrocytic promoter *hGfaABC$_1$D*[47] into the hippocampus of 12- to 14-month-old *Aldh1l1*-CreER^{T2} mice, administered TAM, and performed behavioral analyses 5 weeks thereafter (Figures 2A and S3A). The stringent system featuring two astrocytic promoters enabled inducible, high-efficiency, and cell-type-specific targeting of mGluR3 to hippocampal astrocytes (Figures 2B, 2C, and S3B–S3E). Immunolabeling for mGluR3-HA revealed the characteristic ramified morphology and tiling pattern of hippocampal astrocytes, which is not visible when immunolabeling for GFAP, a cytoskeletal protein that reveals the cell body and larger branches of astrocytes but not their full cell structure.

Intrahippocampal injections of the mGluR3-encoding AAV vectors induced 4-fold increases in mGluR3 immunoreactivity in males and females, with similar coverage in hippocampal subregions across the sexes (Figures 2D and 2E). In primary astrocyte cultures, the AAV vector encoding mGluR3 increased the levels of mGluR3 monomers and functional dimers (Figure S3F),[48,49] and treatment with the mGluR2/3-selective agonist LY354740 increased phosphorylated Akt levels in transduced astrocytes (Figure S3G), demonstrating intact surface expression and signaling by the exogenous receptor.

In the Morris water maze, enhancing astrocytic mGluR3 levels did not affect learning or swim speeds (Figures 2F and S4A–S4E). Although female controls had similar learning to male controls during training, probe trials revealed that female controls had reduced quadrant and crossing index values as compared to age-matched control males at 1 day post-training (Figures 2G and 2H) and 9 days post-training (Figure 2I). Consistent with our observations that partial knockdown of astrocytic mGluR3 impairs performance in females (Figure 1), we found that enhancement of astrocytic mGluR3 improved performance in females, as evidenced by increased target preferences as compared to control females (Figures 2G–2I). In addition, fold change comparisons revealed differential effects of mGluR3 across sexes, further suggesting that mGluR3 induces sex-dependent effects. Of note, although mGluR3 enhanced memory in females, male mice did not have improvements, and there were trends of worsened performance (Figure 2H). Anxiety-like behavior was unaffected in both sexes (Figures S4F and S4G). In control mice without Cre expression, hippocampus-targeted injections of AAV vectors did not affect learning, memory, exploration, or anxiety-like behaviors (Figure S5), indicating that intrahippocampal delivery of AAV vectors was not itself sufficient to alter behavior.

Given the observed differences in probe trial performance in control *Aldh1l1*-CreER^{T2} females as compared to age-matched control *Aldh1l1*-CreER^{T2} males at 12–14 months of age (Figures 2G–2I, see index comparisons), we also examined whether there were intrinsic differences in mGluR3 expression across sexes with age. Hippocampal mGluR3 levels were similar between sexes at 4 and 5–7 months of age (Figures S1F, S3H, and S3I). However, by 12 months of age, mGluR3 levels in the dentate gyrus were increased in males as compared to 4-month-old males and were slightly higher than age-matched females (Figure S3I). By 18 months of age, mGluR3 levels in the dentate gyrus and CA1 region were markedly reduced in both sexes by 35%–40% relative to 4-month-old mice (Figure S3I). These data are consistent with previous reports of gene expression changes with age[50,51] and changes in astrocytic mGluR3 levels in humans and animal models of aging-related neuropathology.[21,23,24] Our findings suggest that hippocampal mGluR3 levels vary substantially with age, which might promote sex-specific effects on hippocampal function.

Modulation of astrocytic mGluR3 has sex-specific effects on search behavior at recall

The hippocampus is one of several brain regions important for spatial navigation and allocentric representations.[52–54] To further examine these aspects of behavior, we performed deeper computational analyses of search patterns in the Morris water maze probe trials. We

focused these analyses on the first 20 s of each trial, representing the most directed search for the target, whereas later time points typically involve extinction processes.[39,55]

We first examined the effects of astrocytic mGluR3 reductions on the accuracy of trajectories during initial approach to the target. Consistent with our findings that mGluR3 knockdown improved target preferences in males and worsened target preferences in females (Figures 1H–1J), mGluR3 knockdown also reduced trajectory errors in males and increased trajectory errors in females (Figure 3A). Fold change comparisons among sexes confirmed differential effects of knockdown on trajectories in males as compared to females. Increases in mGluR3 levels resulted in minimal effects on trajectories (Figure 3B). Thus, reductions in mGluR3 expression in hippocampal astrocytes had sex-dimorphic effects on the accuracy of the initial routes used to find the target during recall trials.

We next examined the frequencies of different types of search strategies used by mice to find the target. In males, astrocytic mGluR3 knockdown increased the frequency of goal-directed search patterns (Figures 3C and 3E), suggesting that males increased their use of allocentric-like strategies, which are often defined by distal cues serving as spatial references for finding a target location rather than the self as the reference. In conjunction, mGluR3 knockdown reduced the total frequency of less-directed, procedural scanning search patterns in males (chaining, scanning, circling), suggesting that males also decreased their usage of potentially more error-prone egocentric strategies, which are defined by fixed or repetitive search patterns based on the self as the reference. Egocentric strategies, which were reduced in male mice with mGluR3 knockdown, are more likely to cause off-target navigation, especially with a changing starting point, which was a feature of the behavioral paradigm. Thus, astrocytic mGluR3 can dampen the accuracy of spatial memory in males and shift search behavior to egocentric patterns.

We did not detect differences in search strategies in males with increased mGluR3 (Figure 3D), consistent with the minimal effects on target preferences (Figures 2G–2I). It is possible that mGluR3 overexpression did not affect performance in males due to a separate, yet-unknown mechanism that enhances performance in males or promotes a period of resilience to these perturbations. Further studies are required to investigate differences in hippocampal astrocyte receptor function in aging and whether certain astrocytic alterations vary by sex and have nonlinear trajectories across lifespan.

In females, unlike males, astrocytic mGluR3 knockdown increased egocentric scanning patterns (Figures 3C and 3E), whereas enhancing mGluR3 levels in females reinstated allocentric, goal-directed search patterns (Figures 3D and 3F). These data suggest that astrocytic mGluR3 enhances the accuracy of spatial memory and promotes allocentric search patterns in females. Strikingly, the effects of reducing mGluR3 in males (Figure 3C) were similar to the effects of increasing mGluR3 in females (Figure 3D), indicating that the receptor has sex-divergent effects on behavior. Trajectory errors and search strategies were not significantly affected in probe trials performed 1 day post-training (Figure S6), possibly because these analyses are more sensitive to remote recall. These complementary computational analyses further suggest that alterations in astrocytic mGluR3 induce sex-

specific effects on memory and contribute to differential neurocognitive changes between sexes.

Stimulation of astrocytic $G_{i/o}$-coupled or G_s-coupled receptors has sex-dimorphic effects on memory

Consistent with our findings, modulation of other astrocytic $G_{i/o}$-coupled receptors[5,6] or chemogenetic stimulation of astrocytic $G_{i/o}$-coupled signaling affects memory in males.[8,9] However, the sex dependence of these effects is not known. We next used chemogenetics to activate astrocytic $G_{i/o}$-coupled signaling and test whether the sex-dependent effects of mGluR3 are unique to this receptor or reflect a broader feature of astrocytic $G_{i/o}$-coupled activities.

We generated an AAV vector encoding Cre-dependent, HA-tagged hM4Di, a $G_{i/o}$-coupled designer receptor exclusively activated by designer drugs (DREADD),[56] under the *hGfaABC$_1$D* promoter (Figure 4A). The vector was delivered to the hippocampus of 4to 7-month-old *Aldh1l1*-Cre mice, which induced robust, astrocyte-selective hM4Di expression (Figures S7A–S7C). mGluR3 and other $G_{i/o}$-coupled receptors affect multiple intracellular cascades, including Akt activation, but induce minimal changes in calcium flux in hippocampal astrocytes, despite clear effects on calcium in the striatum.[14,57–59] To confirm hM4Di activity, we turned to Akt. Stimulation of hM4Di-expressing astrocytes *in vitro* with clozapine-N-oxide (CNO), the synthetic agonist for muscarinic DREADDs, increased phosphorylated Akt (Figures S7D and S7E), indicating functional receptors at the cell surface. Consistent with previous findings,[8] c-Fos levels were increased in hM4Di-expressing astrocytes after *in vivo* delivery of CNO (5 mg/kg, intraperitoneal [i.p.]) (Figure S7F). Drug levels in the hippocampus peaked 1 h after administration (Figure S7G), as reported.[60] Thus, to test if biological sex alters the effects of astrocytic $G_{i/o}$-coupled receptor activity on memory, mice received vehicle or CNO 1 h before training trials (Figure 4B). Hippocampal hM4Di expression was similar between sexes (Figure 4C).

Consistent with the effects of enhancing astrocytic mGluR3 levels, stimulation of hM4Di did not affect learning but did induce sex-specific effects on memory (Figures 4D–4F). Astrocytic hM4Di stimulation with CNO improved target preferences in females (Figures 4E and 4F), akin to enhancing mGluR3, but it reduced target preferences in males (Figure 4F), consistent with findings in males.[8,9] Crossing index and fold change comparisons confirmed differential effects between sexes (Figure 4F). Thus, the sex-specific effects of astrocytic mGluR3 can be recapitulated by stimulating a $G_{i/o}$-coupled receptor, and acute receptor activation in astrocytes during learning is sufficient to induce memory enhancement or impairment, depending on sex. Given that astrocytic mGluR3 and other types of $G_{i/o}$-coupled receptors are expressed throughout the brain,[16,61] we speculate that $G_{i/o}$-coupled signaling may promote sex-specific modulation of various brain functions.

$G_{i/o}$-coupled signaling has convergent and antagonistic interactions with G_s-coupled signaling (Figure S7H). $G_{i/o}$-coupled receptors inhibit cAMP synthesis, whereas G_s-coupled receptors promote cAMP synthesis and can also modulate $G_{i/o}$-coupled cascades.[59,62,63] To further investigate the mechanisms promoting sex-specific effects on memory, we next expressed and activated G_s-coupled DREADDs in hippocampal astrocytes and assessed their

effects on memory. Similar to our hM4Di experiments, we used an AAV vector encoding a Cre-dependent, HA-tagged G_s-coupled DREADD (rM3Ds)[64] under the *hGfaABC$_1$D* promoter for astrocyte-selective targeting (Figure 4G). The mice received vehicle or CNO 1 h before daily training (Figure 4H). Astrocytic expression of rM3Ds was consistent across sexes and restricted to the hippocampus (Figures 4I and S7I–S7K). CNO treatment of rM3Ds-expressing astrocytes *in vitro* increased phosphorylated CREB (Figure S7L), and c-Fos levels were altered in rM3Ds-expressing astrocytes after *in vivo* delivery of CNO (Figure S7M), confirming that astrocytic rM3Ds was functional.

The stimulation of astrocytic rM3Ds during training did not affect learning in males but had a detrimental effect on learning in females, and fold change analyses revealed sex differences in the effects on learning (Figure 4J). Although control females and CNO-treated females reached similar levels of performance at completion of training (Figure 4J), and all controls showed similar quadrant preferences 1 day after training (Figures S8A and S8D), CNO-treated females expressing rM3Ds had impaired performance in the 3-day probe, as reflected by reduced target quadrant and platform preferences and index values (Figures 4K and 4L). Fold change comparisons further pointed to differential responses across sexes (Figures 4K and 4L). Indeed, CNO-treated males had intact target quadrant preferences (Figure 4K) as well as preserved target platform preferences, whereas control males did not show strong preferences (Figure 4L). The stimulation of G_s-coupled or $G_{i/o}$-coupled receptors did not affect swim speeds (Figure S8). The observed memory impairments induced by rM3Ds activation in females were similar to the effects of mGluR3 knockdown and opposite to the effects of hM4Di activation in females, further demonstrating bidirectional and sex-dependent effects. Of note, our results in males are consistent with reports that direct optogenetic stimulation of adenylate cyclase in hippocampal astrocytes improves memory (although sex was not reported)[65] and that astrocytic G_s-coupled adrenergic receptors facilitate memory in males.[3]

CNO is readily converted to clozapine, a psychoactive compound that stimulates endogenous GPCRs.[66] Thus, in additional control experiments, we tested whether CNO had DREADD-independent effects. We found that AAV-injected nontransgenic mice did not have detectable DREADD expression (Figure S9A) and that CNO administration (5 mg/kg, i.p.) during training did not affect performance in either sex (Figures S9B–S9F). Of note, CNO/clozapine is rapidly cleared from the brain within several hours (Figure S7G), whereas the effects on memory in DREADD-expressing mice persisted for several days. Altogether, our findings reveal that biological sex is a key determinant of astrocytic effects on cognitive function.

DISCUSSION

Previous studies have demonstrated sex differences in learning and memory,[46,67–69] neurocognitive disorders,[70] and aging-related cognitive decline,[46] which have been largely attributed to differences in neuronal functions. Although biological sex needs consideration in studies of brain function,[70–73] previous investigations on the cognitive effects of astrocytic receptors have included only male subjects[3,5–12,74,75] or did not report sex differences[4,76] (Table S1). Of note, cortical astrocytes have sex differences in gene expression during brain

development,[77] and hypothalamic astrocytes can induce sex-specific circadian changes.[78] Here, we uncovered sex-dependent behavioral effects across four different manipulations, indicating that astrocytes regulate hippocampal function in a highly sex-specific manner and may contribute to sex differences in behavior.

Increasing astrocytic mGluR3 levels enhanced memory in older females, and reducing mGluR3 was sufficient to impair memory in young females, demonstrating that mGluR3 promotes memory recall in females. In contrast, males had memory improvements upon reductions in mGluR3, whereas increases did not improve memory. In agreement, memory in females was enhanced by the stimulation of $G_{i/o}$-coupled receptors, whereas memory in males was impaired. Conversely, stimulation of G_s-coupled receptors impaired learning and memory in females but not males, implicating astrocytic GPCRs in sex-dimorphic regulation of hippocampal function.

Sex differences in hippocampal function likely involve an interplay of sex-specific mechanisms in astrocytes and other cell types. Astrocytic receptors may induce sex-dimorphic effects by acting on neural circuits with different properties across sexes. For instance, hippocampal neurons in the CA3 have more stable responses to familiar environments during memory retrieval as compared to the CA1,[79] but there are sex differences in baseline CA3-CA1 excitation,[80] with female mice having higher excitation states than males. However, it is also plausible that astrocytes contribute to differential excitation states across sexes. CA3 hyperactivity is associated with aging-related memory loss in rodents[81–83] and humans,[84] and attenuation of CA3 hyperactivity prevents deficits.[85] Older female mice (10–12 months) have increases in synaptophysin labeling in the CA3, whereas males do not have these changes until older ages.[86] Thus, increases in astrocytic mGluR3 might improve memory in females by modulating CA3-CA1 communication. In contrast to females, males with reduced mGluR3 or activation of G_s-coupled rM3Ds had improvements in performance, whereas $G_{i/o}$-coupled hM4Di activation impaired memory. In agreement, activation of astrocytic hM4Di in the CA1 of male mice impairs memory and disrupts CA3-CA1 activities.[8]

mGluR3 reductions also induced divergent effects on path trajectories and search strategies, further implicating this receptor in recall accuracy and shifts in allocentric-egocentric representations. Humans and other animals use allocentric and egocentric strategies together, likely for robust spatial representations and flexible navigation, although species-related differences are possible. Egocentric representations involve the postrhinal and retrosplenial cortices, and these representations can be transformed into allocentric representations,[87–89] but the exact mechanisms and roles of glial cells in these processes are not known. Our findings implicate astrocytic GPCRs as sex-specific modulators of spatial representations, possibly through effects on hippocampal-neocortical communication.

Chemogenetic manipulations revealed that astrocytic regulation of memory involves a sex-specific balance between G_s-coupled and $G_{i/o}$-coupled receptor signaling and that alterations in this balance have sex-divergent effects. Although some signaling factors have been linked to sex-specific effects,[90–93] the exact mechanisms by which receptor signaling pathways diverge are not yet known. Astrocytic receptors may also engage sex-dependent

mechanisms in neurons that result in distinct behavioral outcomes in a non-cell-autonomous manner.[67,69,80,94,95]

GPCRs and related factors are the largest family of proteins targeted by approved drugs, and mGluR3 modulators are being developed for clinical applications. Our study suggests that targeting mGluR3 and other astrocytic GPCRs may cause sex-specific neurocognitive effects. Astrocytic GPCRs are altered in various disorders[4,21,23,24,74,96–98] and might contribute to sex differences in disease, an important consideration in personalized medicine.[70,99] Our results support an emerging view that astrocytes induce context-dependent changes and contribute to selective vulnerability.[100] Astrocytic signaling can modulate diverse brain regions and functions, including glutamatergic[19,35,58] and GABAergic transmission,[61,76] suggesting that a spectrum of activities might be subject to sex-dependent regulation.

Limitations of the study

The present study used transgenic mice to examine astrocytic GPCRs. It remains unclear how these findings translate across species and if they apply to other types of astrocytic signaling pathways and brain regions. Further studies are needed to determine the relevance of these findings to aging- and disease-related alterations in cognitive processes, which are associated with astrocytic changes and sex-dependent outcomes.[101,102] Additional work is required to define the exact molecular and neural circuit mechanisms and evaluate the potential roles of circulating sex hormones and sex chromosomes in the observed effects.

STAR★METHODS

RESOURCE AVAILABILITY

Lead contact—Further information and requests for resources and reagents should be directed to the lead contact, Anna G. Orr (ago2002@med.cornell.edu).

Materials availability—Plasmids generated in this study are available from the lead contact but may require a completed materials transfer agreement.

Data and code availability

- All raw data reported in this paper are available upon request from the lead contact.
- This paper does not report original code.
- Any additional information required to reanalyze the data reported in this work is available from the lead contact upon request.

EXPERIMENTAL MODEL AND SUBJECT DETAILS

Animals—All animal experiments were approved by the Institutional Animal Care and Use Committee of Weill Cornell Medicine and conducted in accordance with the guidelines set by the National Institutes of Health Guide for the Care and Use of Laboratory Animals. Mice were group-housed, with two to four mice per cage. Mice were maintained on a 12-h

light/dark cycle with *ad libitum* access to food and water. All experiments were conducted during the light cycle and included littermate controls. In consideration of sex as a biological variable, all experiments were conducted to power each treatment group for both sexes at 80% power, with α set at 0.05. Although circulating hormone levels and estrous cycles were not monitored, we did not observe segmentation in the data and effects were typically consistent across multiple probe trials in the Morris water maze.

Astrocyte-targeted knockdown of mGluR3 was achieved using *Aldh1l1*-CreER^{T2} BAC transgenic mice crossed with Rosa26-LSL-Cas9-eGFP knock-in mice (*Aldh1l1*-CreER^{T2} x Rosa26-LSL-Cas9-eGFP). *Aldh1l1*-CreER^{T2} mice (Jackson Laboratory; strain #031008) express tamoxifen (TAM)-inducible Cre recombinase under the control of the astrocytic aldehyde dehydrogenase 1 family member L1 (*Aldh1l1*) promoter (kindly provided by Dr. Baljit S. Khakh). Rosa26-LSL-Cas9 mice (Jackson Laboratory; strain #026556) have Cre recombinase-dependent expression of the CRISPR-associated protein 9 (Cas9) endonuclease and eGFP under the CAG promoter. Use of Rosa26-LSL-Cas9-eGFP mice in combination with sgRNA vectors and a source for Cre recombinase enables manipulation of gene expression. The resulting *Aldh1l1*-CreER^{T2} x Rosa26-LSL-Cas9-eGFP cross enabled induction of Cas9 and eGFP expression selectively in astrocytes. Mice did not express Cas9-eGFP until treatment with TAM.

Astrocyte-targeted enhancement of mGluR3 expression was achieved using singly transgenic *Aldh1l1*-CreER^{T2} mice. One to two weeks post-stereotaxic injections, mice received single daily injections of TAM (MilliporeSigma, 80 mg/kg, i.p.) for five consecutive days. Notably, TAM is a known estrogen receptor modulator that can facilitate estrogen receptor degradation and act as a mixed agonist and antagonist that might affect behavior. However, short-term TAM administration does not alter EPM or Morris water maze performance in either sex.[105] Nonetheless, we designed our experiments to minimize potential interactions between our manipulations and TAM administration. In *Aldh1l1*-CreER^{T2} mice with mGluR3 manipulations, all behavioral experiments were performed no less than five weeks after cessation of TAM administration. TAM and its psychoactive metabolites are minimally detectable by one week after administration.[106] We conclude that there was minimal direct influence of TAM on the behavioral measurements in our study. The sex-specific effects observed with the mGluR3 manipulations were recapitulated with chemogenetic stimulation using independent mouse lines and AAV vectors. The chemogenetic experiments were conducted in *Aldh1l1*-Cre mice that were not exposed to TAM.

The expression of chemogenetic receptors hM4Di and rM3Ds was targeted to astrocytes using *Aldh1l1*-Cre mice (B6; FVB-Tg(Aldh1l1-cre)JD1884Htz/J). *Aldh1l1*-Cre mice were obtained from the Jackson Laboratory (strain #023748) and backcrossed for five generations onto the C57Bl/6J background. Similar to *Aldh1l1*-CreER^{T2} mice, *Aldh1l1*-Cre mice express Cre recombinase downstream of the astrocytic *Aldh1l1* promoter, but there is no dependence on TAM. Behavioral studies were conducted 3–5 weeks after stereotaxic injections.

Primary astrocyte cultures—All cultures were maintained at 37°C in a humidified 5% CO_2-containing atmosphere. Cortices and hippocampi from postnatal day 3 mouse pups (nontransgenic or *Aldh1l1*-Cre) were cleared of meninges, dissociated by manual trituration with a P1000 pipette, and plated into culture plates pre-coated with poly-D-lysine (50 μg/mL, MilliporeSigma). Cells were maintained in DMEM supplemented with 20% heat-inactivated FBS (VWR #89510–188), 1X GlutaMAX (ThermoFisher #35050061) and 1 mM sodium pyruvate (Thermo Scientific). Cells were washed after 4–5 days in culture and maintained in fresh media after washing. After 9–11 days in culture, medium was replaced with DMEM without serum and glutamine, and cells were treated 18–24 h later with clozapine-N-oxide (CNO, Tocris #4936, 5 μM) or LY354740 (Tocris #3246, 1 μM) for 10 min prior to lysis to assess the levels of phosphorylated and total proteins by Western blotting.

METHOD DETAILS

Adeno-associated viral vectors (AAVs)—To knock down mGluR3, AAV vectors were generated by removing the human synapsin promoter and mCherry sequences from pAAV-*U6*-sgRNA-hSyn-mCherry vector (donated by Dr. Alex Hewitt, Addgene #87916; RRID #Addgene 87916)[103] using Anza 32 ApaI and Anza 14 SalI (Thermo Fisher Scientific) and the plasmid backbone was ligated with Anza T4 DNA Ligase Mix to create pAAV-*U6*-sgRNA. The existing 20 bp sgRNA spacer sequence was removed using Anza 33 LguI. sgRNAs targeting mouse *Grm3* were designed[107] and ordered as pairs of complementary unphosphorylated oligos (Integrated DNA Technologies):

#552 forward, CACCGCAGAGGTATCCAACGCCTGG;

#552 reverse, AAACCCAGGCGTTGGATACCTCTGC;

#703 forward, CCGCAGAGCATCGTTGACTAAAG;

#703 reverse, AACCTTTAGTCAACGATGCTCTGC.

Oligo pairs were phosphorylated, annealed, and ligated into the LguI-digested backbone to generate two AAV vectors.

To enhance mGluR3 expression levels, the truncated human astrocyte-specific *GfaABC1D* promoter was digested from pAAV-*GFAP*-EGFP (donated by Dr. Bryan Roth, Addgene #50473; RRID #Addgene_50473) and cloned into pAAV-*EF1a*-DIO-hM4D(Gi)-mCherry (donated by Dr. Bryan Roth, Addgene #50461; RRID #Addgene_50461) using Anza 28 MluI and Anza 14 SalI to replace the *EF1a* promoter. Rat mGluR3 with an N-terminal HA tag was synthesized as a gene block (Integrated DNA Technologies) and ligated in place of the hM4D(Gi) sequence of pAAV-*GfaABC1D*-DIO-hM4D(Gi)-mCherry using Anza 6 NheI and Anza 21 SgsI. To reduce construct size, the human growth hormone (hGH) poly-adenylation (polyA) sequence was replaced with the shorter bovine growth hormone (bGH) polyA sequence PCR amplified (Platinum SuperFi DNA Polymerase kit, ThermoFisher #12351010) from pCRII-TOPO *CMV*-cGFP-bGH Poly(A) (donated by Dr. Phil Sharp, Addgene #46835; RRID #Addgene_46835)[104] using primers containing XhoI and CpoI

restriction sites. The resulting construct enabled Cre-dependent expression of mGluR3 in astrocytes. Control experiments involved injection of AAV vectors into nontransgenic mice.

For chemogenetic experiments, the $G_{i/o}$-coupled chemogenetic receptor hM4Di was PCR amplified from pAAV-*GFAP*-HA-hM4D(Gi)-IRES-mCitrine (donated by Dr. Bryan Roth, Addgene #50471; RRID #Addgene_50471) using primers containing NheI and SgsI restriction sites in order to replace the HA-mGluR3 sequence in the pAAV-*GfaABC1D*-DIO-HA-mGluR3 construct to generate pAAV-*GfaABC1D*-DIO-HA-hM4D(Gi) for Cre-dependent expression of HA-tagged hM4Di in astrocytes. Similar methods were employed to amplify the G_s-coupled chemogenetic receptor rM3D(Gs) from pAAV-*GFAP*-HA-rM3D(Gs)-IRES-mCitrine (donated by Dr. Bryan Roth, Addgene Plasmid #50472; RRID #Addgene_50472) to generate pAAV-*GfaABC1D*-DIO-HA-rM3D(Gs) for Cre-dependent expression of HA-tagged rM3Ds in astrocytes.

All vectors were transformed into NEB 5-alpha competent bacteria (New England Biolabs #C2987H) and purified with the Plasmid Plus Maxi Prep kit (Qiagen #12963). The integrity and accuracy of each AAV vector, including both AAV-ITRs, were verified by restriction digests and Sanger sequencing (Genewiz and Azenta) prior to viral production. AAV2/PHP.eB viral particles were produced by the Stanford University Gene Vector and Virus Core (sgRNA vectors) and the University of Pennsylvania (mGluR3, hM4Di, and rM3Ds). PHP.eB capsid vectors were provided courtesy of Drs. Viviana Gradinaru and Benjamin Deverman at the California Institute of Technology.[32,33] PHP capsids are a modification of AAV9 provided by the University of Pennsylvania.

Stereotaxic surgeries—Prior to surgery, mice were anesthetized with Avertin (2,2,2-tribromoethanol; Fisher Scientific #AC421430100, 200 mg/kg, i.p.) and supplemented with inhalant isoflurane (1%, Covetrus). During surgeries, meloxicam (2 mg/kg, s.c., Covetrus) and bupivacaine (1 mg/kg, t.d., Hospira) were administered for pain management. Once anesthetized, mice were secured in a stereotaxic frame (Kopf Instruments) and bilateral 1 mm-diameter openings were made in the skull using a mounted drill (Kopf Instruments). A 10 μL Hamilton syringe mounted to the stereotaxic frame was used to infuse 1 μL of sgRNAs (1:1 mixture of AAV2/PHP.eB-*U6*-sgRNA552 (4.09×10^{12} viral genomes (Vg)/mL) and AAV2/PHP.eB-*U6*-sgRNA703 (2.11×10^{12} Vg/ml)), or 0.5 μL AAV2/PHP.eB-*hGfaABC1D*-DIO-HA-mGluR3 (8.15×10^{12} Vg/ml), or 0.5 μL AAV2/PHP.eB-*hGfaABC1D*-DIO-HA-hM4Di (1.12×10^{13} Vg/ml), or 0.5 μL AAV2/PHP.eB-*hGfaABC1D*-DIO-HA-rM3Ds (1.83×10^{13} Vg/ml) into the dorsal hippocampus at the following stereotaxic coordinates (relative to bregma): −2.3 anterior/posterior; +/−2.0 medial/lateral; −2.0 dorsal/ventral. All AAV vectors were injected using a Micro 4 Microsyringe Pump (World Precision Instruments) at a rate of 0.1 μL/min. After each injection, the needle was left in place for an additional 5 min to allow for diffusion of the AAV. After needle withdrawal, the surgical site was sealed with Vetbond tissue adhesive (3M), and mice were continuously monitored under a heating lamp until fully recovered.

Retro-orbital injections—To confirm DREADD functionality *in vivo*, *Aldh1l1*-Cre mice were injected retro-orbitally with AAV2/PHP.eB vectors. Mice were briefly anesthetized with isoflurane (3%, Covetrus) and injected with 100 μL AAV2/PHP.eB-*hGfaABC1D*-DIO-

HA-hM4Di (1×10^{11} Vg/mouse) or AAV2/PHP.eB-*hGfaABC1D*-DIO-HA-rM3Ds (1×10^{11} Vg/mouse) diluted in saline into the retro-orbital sinus. Petrolatum ophthalmic ointment (Puralube Vet Ointment) was applied to the injected eye and mice were allowed to recover for three weeks before receiving vehicle or CNO (i.p., 5 mg/kg), followed by perfusion and processing for tissue immunolabeling.

Behavioral testing—Age-matched littermates were distributed across experimental groups in home cages of each sex. Experimenters were blinded to experimental groups and mice were tested in random order. Before behavioral testing, except for the elevated plus maze, all mice were handled for 1–2 min per day for 5 days. Mice that were injured or in poor health were excluded from behavioral testing, regardless of experimental group. Prior to all behavioral tests, mice were acclimated to the testing room and lighting for 1 h. For experiments involving mGluR3 manipulations, behavioral testing began 5–6 weeks after completion of TAM administration and the elevated-plus maze testing was performed prior to the Morris water maze experiments. For chemogenetic experiments, behavioral testing began 3–5 weeks after stereotaxic injections.

Elevated plus maze—The elevated plus maze is a raised plus-shaped maze consisting of two enclosed arms and two open arms. The maze is raised 60–70 cm above the ground and placed under bright white light. After habituation to the room, the mice were placed in an open arm facing the center of the maze. Mice were allowed to freely explore the four arms of the plus-shaped maze for 5 min. The trial period was recorded and tracked using EthoVision XT video tracking software (Noldus Information Technology Inc., Leesburg VA). Between mice, the maze was cleaned with 70% ethanol to avoid interference between trials.

Morris water maze—Mice were tested in a 122 cm diameter pool filled with room temperature water (20 ± 2°C). The water was made opaque with white tempera paint (Colorations Non-Toxic Liquid Paint). Prior to testing, geometric spatial cues were set up around the pool. On the first day, mice underwent one session of three pre-training trials wherein mice were placed at one end of a rectangular channel (15 cm × 122 cm) with a square platform (14 × 14 cm) submerged 0.5 cm below the surface of the water at the other end of the channel. If a mouse did not swim to the channel within 15 s, the mouse was guided onto the platform, where it remained for 10 s before being gently dried and returned to the home cage. Three days following pre-training, the mice underwent hidden platform training in the full circular water maze.

During hidden platform training, the platform was submerged approximately 1.0 cm below the surface of the water. Training consisted of one session per day for 5–7 consecutive days. In each training session, mice completed four training trials, wherein the drop location was varied but the platform location remained the same. The maximum trial time was 60 s. If the mouse did not find the platform within 60 s, it was gently guided to the platform by the experimenter. All mice sat on the target platform for 10 s after each training trial. During DREADD experiments, mice received injections of vehicle (0.5% DMSO in 0.9% saline, i.p.) or clozapine-N-oxide (CNO, Tocris #4936; 5 mg/kg, i.p.) 1 h prior to each training session. As shown in Figure 4, mice in the rM3Ds experiment were trained for an extra day

as compared to mice in the hM4Di experiment because overall learning was slower for all groups in the rM3Ds-related training trials and females had reduced learning.

During the probe trials, the hidden platform was removed from the pool and each mouse underwent one 60 s trial on each probe day, with the drop location kept constant at 180° angle from the target platform location. At the end of each trial, mice were removed from the pool, dried off to minimize stress, and placed back in the home cage.

Environmental or handling-related stress is known to affect behavioral readouts. Unlike mice that underwent mGluR3 manipulations, the mice used in chemogenetic experiments underwent daily intraperitoneal injections 1 h prior to training, which can cause stress and impair learning, accelerate the rate of forgetting, and affect probe performance in all groups.[108–110] Thus, for chemogenetic experiments, we performed probe trials at one and three days post-training rather than one and nine days post-training. Similar trends of sex-specific effects of hM4Di and rM3Ds stimulation were observed in probe trials at one day post-training.

Rtrack analyses—Raw data were exported from Ethovision XT and processed and analyzed using R (version 4.0.3). Search strategies during the training trials were determined from search patterns during the entire 60 s trial, as previously reported.[111] Each individual probe trial was truncated to include only the first 20 s of the probe trial as previous studies have reported that this initial search period is the most sensitive to memory deficits during probe trials.[39,55] The *Rtrack* package (version 1.0.0)[40] was used to determine the confidence score (percent match as a measurement of how well the swim path fit each model) for nine predefined swim strategies: non-goal-oriented strategies (thigmotaxis, circling, random), procedural strategies (scanning, chaining), and allocentric strategies (goal-directed search, corrected search, direct path, perseverance). Rtrack designers recommend a cutoff threshold of 0.4 for calling strategy.[40] To maximize data inclusion, we did not set a threshold for confidence scores. Confidence scores ranged from 0.276 to 0.744 (64% over 0.4) for probe data in the sgRNA experiment, and from 0.218 to 0.80 (84% over 0.4) for probe data in the mGluR3 AAV experiment. Data are shown as the percentage of mice that utilized each swim strategy during a trial.

Rtrack was also used to calculate the initial trajectory error in each probe trial. This calculation assesses the distance of the mouse from the center of the goal (target platform) after a total swim distance equivalent to the calculated distance of a direct swim path from the starting point to the goal. This measure serves as a measure of the accuracy of the initial swim path.

Immunohistochemistry—Mice were anesthetized with Avertin (250 mg/kg, i.p.) and transcardially perfused for 3 min with 0.9% saline. Brains were removed and drop-fixed in PBS-buffered 4% paraformaldehyde (PFA) for 24 h, then rinsed three times with PBS before equilibrating with PBS-buffered 30% sucrose at 4°C until sectioning (at least 24 h). Mouse brains were sectioned at a thickness of 30 μm using an SM2010 R sliding microtome (Leica) equipped with a BFS-3MP freeing stage and cooling unit (Physitemp, Clifton, NJ).

Free-floating sections were collected and stored in cryopreservative (30% ethylene glycol, 30% glycerol in PBS) for long-term storage at −20°C.

For all immunolabeling, free-floating sections were rinsed in PBS and permeabilized in PBS containing 0.5% Triton X-100 (PBS-T). Sections were blocked with 6% goat and/or donkey serum (Jackson ImmunoResearch) in PBS-T for 1–2 h at room temperature. Blocked sections were rinsed in PBS and incubated for 24 h (or for 48 h for Iba1 labeling) at 4°C in mouse anti-HA (1:500, 901513, Biolegend, RRID#AB_2565335), rabbit anti-HA (1:1000, 3724S, Cell Signaling, RRID#AB_1549585), rabbit anti-GFAP (1:1,000, G9269, MilliporeSigma, RRID#AB_477035), mouse anti-GFAP (1:1,000, MAB3402B, MilliporeSigma, RRID#AB_10917109), goat anti-GFAP (1:500, ab53554, Abcam, RRID# AB_880202), chicken anti-GFAP (1:1000, ab4674, Abcam, RRID#AB_304558), rabbit anti-mGluR3 (1:500, ab166608, Abcam, RRID#AB_2833092), chicken anti-GFP (1:500, ab13970, Abcam, RRID#AB_300798), rabbit anti-NeuN (1:1000, ABN78, MilliporeSigma, RRID#AB_10807945), guinea pig anti-NeuN (1:2500, ABN90, MilliporeSigma, RRID#AB_11205592), mouse anti-*c*-Fos (1:1,000, ab208942, Abcam, RRID# AB_2747772), or goat anti-Iba1 (1:400, ab5076, Abcam, RRID#AB_222402 diluted in 3% serum in PBS-T.

Sections were rinsed and incubated for 1–2 h at room temperature in AlexaFluor-conjugated secondary antibodies diluted 1:500 (ThermoFisher Scientific #A-31573, A-31572, A-31571, A-31570, A-21432, A-21206, A-21202, A-78949, A-21447, RRID#AB_2536183, AB_162543, AB_162542, AB_2536180, AB_2535853, AB_2535792, AB_141607, AB_2921071, RRID:AB_141844; Abcam ab150169, RRID# 2636803; Jackson ImmunoResearch # 706–605-148, RRID#AB_2340476) and in DAPI (D9542, Millipore-Sigma) diluted 1:3,000 in 3% serum in PBS-T before final rinses with PBS. Sections were mounted onto Superfrost slides (VWR), and coverslips were mounted with Vectashield (Vector Labs) or Prolong Diamond media (ThermoFisher Scientific).

Most images were acquired using a BX710 microscope (Keyence) with a 10X or 20X objective (Nikon), stitched with BZ-X Analyzer Software (Keyence), and analyzed with ImageJ (FIJI). For measuring mGluR3 expression, images were captured using an LSM880 confocal microscope (Zeiss) equipped with 20X objectives (Zeiss). Images were processed in Zen Black v2.3 SP1 FP3 acquisition software (Zeiss) to create maximum intensity projection of z stack overlays. Images were processed in FIJI to create z stack overlays of representative fields.

For determining specificity and efficiency of vector targeting, brightness and contrast of thresholded images were adjusted to better visualize immunolabeling of cell markers, receptors, and/or Cas9-eGFP in individual cells and manual counts were performed using the Cell Counter plugin in FIJI. EGFP-positive astrocytes were classified based on their characteristic diffuse, bushy appearance overlapping with intense GFAP labeling which typically only reveals primary processes but not the full morphology. Neurons and microglia/macrophages were classified based on NeuN and Iba1 labeling, respectively. To be classified within these cell types, receptor or Cas9-eGFP labeling had to be centered over NeuN- or Iba1-positive soma and/or show the characteristic morphology of neurons or

microglia. All colocalization counts were performed manually across 2–4 ROIs or images per brain region and mouse. Experimenters were blinded to sample identity.

For measurements of mGluR3 expression, 2–3 ROIs per brain region and mouse were extracted and thresholded to exclude background signal before quantification for mean intensity and percent of total area. Mean mGluR3 intensity was normalized to the ROI area. The levels of endogenous mGluR3 expression appear low in Figure 2B due to the low exposure settings required to capture the higher levels of mGluR3 in AAV-injected mice without saturating the signal. Images included in Figure S3B show that endogenous mGluR3 expression is robust in control mice after adjusting the exposure settings. For measurements of c-Fos levels, HA-positive areas representing DREADD expression were selected as ROIs to restrict these analyses to DREADD-expressing astrocytes.

Microfluidic RT-qPCR—Saline-perfused brain tissue was flash frozen in isopentane on dry ice and stored at −80°C until dissection. Briefly, frozen hemibrains were affixed in warm 30% low-melting point agarose and rapidly cut to 450 μm sections using the McIlwain Tissue Chopper (Stoelting #51350). The sections were quickly placed in ice-cold PBS and the dentate gyrus and the hippocampal CA1 region were dissected under a dissecting microscope (AmScope), placed in RNase-free low-binding tubes (Eppendorf), and re-frozen on dry ice until storage at −80°C. Dissected tissue was homogenized in extraction buffer (Qiagen RLT with β-mercaptoethanol) in a pre-chilled adaptor tube rack using a Fisherbrand Bead Mill 24 (Fisher Scientific #15–340-163) for 20 s with speed setting 5.

RNA was purified using the RNeasy Mini Kit with on-column DNase treatment following manufacturer's instructions (Qiagen #74106, #79256), denatured for 5 min at 70°C and reverse transcribed with the Protoscript First Strand Synthesis Kit (New England Biolabs #6300L). cDNA was pre-amplified for 14 cycles against a pool of selected primers (Table S4) using PreAmp Grandmaster mix (TATAA Biocenter, Sweden #TA05). Pre-amplified DNA underwent exonuclease I treatment (New England Biolabs #M0293L) before being diluted 10-fold with nuclease-free water and mixed with SsoFast EvaGreen with Low ROX (BioRad #1725211). Samples were mixed with chip-specific reagents (Standard BioTools) and then loaded into a 96.96 Dynamic Array Chip (BMK-M-96.96). The chip inlets were loaded with individual primers pre-mixed with DNA assay reagent (Standard BioTools). The IFC Controller HX was used to prime and load the chip in preparation for qPCR. Amplification and melting curves were measured and analyzed with the BioMark HD System (Standard BioTools). Cycle of quantification (Cq) values were thresholded by the BioMark software and normalized to the average of reference genes (*Actb*, *Gapdh*, *Gusb*, *Tbp*). Normalized Cq values were then used to determine the ddCq and fold change relative to control groups.

Western blotting—Cultured astrocytes were rinsed with ice-cold PBS before aspirating buffer and lysing on ice for 10 min with ice-cold buffer containing 10 mM Tris (pH 7.4), 150 mM NaCl, 0.5% deoxycholate, 5 mM EDTA, 0.5% Triton X-100, protease inhibitor cocktail (Roche #11836153001), and two phosphatase inhibitor cocktails (MilliporeSigma P5726 and P0044). Harvested lysates were sonicated on ice for 5 s at 10% power with a probe sonifier (Branson), centrifuged at 10,000 rpm for 10 min at 4°C, and the supernatants

assayed for protein content (Pierce Detergent-Compatible Bradford Assay, ThermoFisher #23246).

Samples (10–20 mg/well) were separated using 4–12% NuPAGE Bis-Tris gels (ThermoFisher #NP0336BOX) and transferred to nitrocellulose membranes using a Mini Blot Module (ThermoFisher). Membranes were blocked for 1 h in 5% bovine serum albumin (BSA) (VWR #97062–904) in Tris-buffered saline prior to incubation overnight at 4°C in 3% BSA in TBS containing 0.2% Tween 20 (TBS-T) and the following primary antibodies: rabbit anti-phospho-CREB (S133) (1:1000, Cell Signaling 9198, RRID#AB_2561044) and mouse anti-total-CREB (1:250, Cell Signaling 9104S, RRID#AB_490881), rabbit anti-phospho-Akt (Ser473) (1:2500, Abcam ab81283, RRID#AB_2224551) and mouse anti-total-Akt (1:250, Cell Signaling 2920S, RRID#AB_1147620), or rabbit anti-mGluR3 (1:500, Abcam ab166608, RRID#AB_2833092) and mouse anti-γ-tubulin (1:2500, MilliporeSigma T5326, RRID#AB_532292).

After washing, membranes were incubated in IR Dye 680RD donkey anti-mouse (1:15,000; LI-COR #926–68072, RRID#AB_2814912) and IR Dye 800CW donkey anti-rabbit (1:15,000; LI-COR #926–32213; RRID#AB_621848) in 3% BSA in TBS-T for 1 h. Blots were rinsed twice with TBS-T and once with TBS and then dried before imaging on the Odyssey CLx scanner (Licor). Immunoblotting was quantified using LI-COR Image Studio software.

Pharmacokinetic analyses—Clozapine and CNO measurements in brain tissue were performed by Charles River Laboratories (South San Francisco, US). Analytes were extracted from pre-weighed hippocampal tissue using standard methods and quantified by LC-MS/MS against analyte calibration curves.

QUANTIFICATION AND STATISTICAL ANALYSIS

Statistical specifications are reported in the figures and corresponding figure legends. Numbers of mice used in each experiment are listed in Tables S2 and S3. All data are presented as mean ± S.E.M, unless indicated otherwise in the legends. Statistical tests were performed using GraphPad Prism 8 or 9. The criterion for data point exclusion was established during the design of the study and was set to values above or below two standard deviations from the group mean. For determination of target preferences, mice with thigmotaxis were excluded. Two-sided Student’s t-tests were used to determine statistical significance between two groups. Welch’s correction was used to account for unequal variances. Differences among multiple groups were assessed by one-way, two-way, or three-way ANOVAs followed by Sidak’s multiple comparisons post-hoc tests, as specified in the legends. Fisher’s exact test was used to compare strategy frequencies across groups. Null hypotheses were rejected at $p < 0.05$.

Supplementary Material

Refer to Web version on PubMed Central for supplementary material.

ACKNOWLEDGMENTS

We thank S. Tymchuk and M.A. Fatafta for technical assistance; M. Garvey, G. Coronas-Samano, L.J. Metakis, and E. Spencer for administrative assistance; T.A. Milner, A. Rajadhyaksha, K. Pleil, and O. Boudker for project guidance; B. Khakh for *Aldh1l1*-CreER^{T2} BAC mice; and the Weill Cornell Microscopy and Imaging Core for support. Schematics were generated using BioRender.com. This work was funded by the National Institutes of Health: R00AG048222 and RF1NS118569 (A.G.O.), and T32GM007739 to the Tri-Institutional MD-PhD Program (C.Z.); the National Science Foundation: 191335 (S.M.M.); the Alzheimer's Association: AARG-17–533273 (A.G.O.); and the Leon Levy Foundation (A.G.O.).

REFERENCES

1. Nagai J, Yu X, Papouin T, Cheong E, Freeman MR, Monk KR, Hastings MH, Haydon PG, Rowitch D, Shaham S, and Khakh BS (2021). Behaviorally consequential astrocytic regulation of neural circuits. Neuron 109, 576–596. 10.1016/j.neuron.2020.12.008. [PubMed: 33385325]
2. Santello M, Toni N, and Volterra A (2019). Astrocyte function from information processing to cognition and cognitive impairment. Nat. Neurosci. 22, 154–166. 10.1038/s41593-018-0325-8. [PubMed: 30664773]
3. Gao V, Suzuki A, Magistretti PJ, Lengacher S, Pollonini G, Steinman MQ, and Alberini CM (2016). Astrocytic beta2-adrenergic receptors mediate hippocampal long-term memory consolidation. Proc. Natl. Acad. Sci. USA 113, 8526–8531. 10.1073/pnas.1605063113. [PubMed: 27402767]
4. Orr AG, Hsiao EC, Wang MM, Ho K, Kim DH, Wang X, Guo W, Kang J, Yu GQ, Adame A, et al. (2015). Astrocytic adenosine receptor A2A and Gs-coupled signaling regulate memory. Nat. Neurosci. 18, 423–434. 10.1038/nn.3930. [PubMed: 25622143]
5. Han J, Kesner P, Metna-Laurent M, Duan T, Xu L, Georges F, Koehl M, Zhang X, Abrous DN, Mendizabal-Zubiaga J, et al. (2012). Acute Cannabinoids Impair Working Memory through Astroglial CB1 Receptor Modulation of Hippocampal LTD. Cell 148, 1039–1050. 10.1016/j.cell.2012.01.037. [PubMed: 22385967]
6. Robin LM, Oliveira da Cruz JF, Langlais VC, Martin-Fernandez M, Metna-Laurent M, Busquets-Garcia A, Bellocchio L, Soria-Gomez E, Papouin T, Varilh M, et al. (2018). Astroglial CB1 Receptors Determine Synaptic D-Serine Availability to Enable Recognition Memory. Neuron 98, 935–944.e5. 10.1016/j.neuron.2018.04.034. [PubMed: 29779943]
7. Adamsky A, Kol A, Kreisel T, Doron A, Ozeri-Engelhard N, Melcer T, Refaeli R, Horn H, Regev L, Groysman M, et al. (2018). Astrocytic Activation Generates De Novo Neuronal Potentiation and Memory Enhancement. Cell 174, 59–71.e14. 10.1016/j.cell.2018.05.002. [PubMed: 29804835]
8. Kol A, Adamsky A, Groysman M, Kreisel T, London M, and Goshen I (2020). Astrocytes contribute to remote memory formation by modulating hippocampal-cortical communication during learning. Nat. Neurosci. 23, 1229–1239. 10.1038/s41593-020-0679-6. [PubMed: 32747787]
9. Jones ME, Paniccia JE, Lebonville CL, Reissner KJ, and Lysle DT (2018). Chemogenetic Manipulation of Dorsal Hippocampal Astrocytes Protects Against the Development of Stress-enhanced Fear Learning. Neuroscience 388, 45–56. 10.1016/j.neuroscience.2018.07.015. [PubMed: 30030056]
10. Van Den Herrewegen Y, Sanderson TM, Sahu S, De Bundel D, Bortolotto ZA, and Smolders I (2021). Side-by-side comparison of the effects of Gq- and Gi-DREADD-mediated astrocyte modulation on intracellular calcium dynamics and synaptic plasticity in the hippocampal CA1. Mol. Brain 14, 144. 10.1186/s13041-021-00856-w. [PubMed: 34544455]
11. Li WP, Su XH, Hu NY, Hu J, Li XW, Yang JM, and Gao TM (2022). Astrocytes Mediate Cholinergic Regulation of Adult Hippocampal Neurogenesis and Memory Through M1 Muscarinic Receptor. Biol. Psychiatr. 92, 984–998. 10.1016/j.biopsych.2022.04.019.
12. Jensen CJ, Demol F, Bauwens R, Kooijman R, Massie A, Villers A, Ris L, and De Keyser J (2016). Astrocytic beta2 Adrenergic Receptor Gene Deletion Affects Memory in Aged Mice. PLoS One 11, e0164721. 10.1371/journal.pone.0164721. [PubMed: 27776147]
13. Tanabe Y, Nomura A, Masu M, Shigemoto R, Mizuno N, and Nakanishi S (1993). Signal transduction, pharmacological properties, and expression patterns of two rat

metabotropic glutamate receptors, mGluR3 and mGluR4. J. Neurosci. 13, 1372–1378. 10.1523/JNEUROSCI.13-04-01372.1993. [PubMed: 8463825]

14. Sun W, McConnell E, Pare JF, Xu Q, Chen M, Peng W, Lovatt D, Han X, Smith Y, and Nedergaard M (2013). Glutamate-dependent neuroglial calcium signaling differs between young and adult brain. Science 339, 197–200. 10.1126/science.1226740. [PubMed: 23307741]
15. Zhang Y, Chen K, Sloan SA, Bennett ML, Scholze AR, O'Keeffe S, Phatnani HP, Guarnieri P, Caneda C, Ruderisch N, et al. (2014). An RNA-sequencing transcriptome and splicing database of glia, neurons, and vascular cells of the cerebral cortex. J. Neurosci. 34, 11929–11947. 10.1523/JNEUROSCI.1860-14.2014. [PubMed: 25186741]
16. Endo F, Kasai A, Soto JS, Yu X, Qu Z, Hashimoto H, Gradinaru V, Kawaguchi R, and Khakh BS (2022). Molecular basis of astrocyte diversity and morphology across the CNS in health and disease. Science 378, eadc9020. 10.1126/science.adc9020. [PubMed: 36378959]
17. Planas-Fontanez TM, Dreyfus CF, and Saitta KS (2020). Reactive Astrocytes as Therapeutic Targets for Brain Degenerative Diseases: Roles Played by Metabotropic Glutamate Receptors. Neurochem. Res. 45, 541–550. 10.1007/s11064-020-02968-6. [PubMed: 31983009]
18. Kellner V, Kersbergen CJ, Li S, Babola TA, Saher G, and Bergles DE (2021). Dual metabotropic glutamate receptor signaling enables coordination of astrocyte and neuron activity in developing sensory domains. Neuron 109, 2545–2555.e7. 10.1016/j.neuron.2021.06.010. [PubMed: 34245686]
19. Egan MF, Straub RE, Goldberg TE, Yakub I, Callicott JH, Hariri AR, Mattay VS, Bertolino A, Hyde TM, Shannon-Weickert C, et al. (2004). Variation in GRM3 affects cognition, prefrontal glutamate, and risk for schizophrenia. Proc. Natl. Acad. Sci. USA 101, 12604–12609. 10.1073/pnas.0405077101. [PubMed: 15310849]
20. Fallin MD, Lasseter VK, Avramopoulos D, Nicodemus KK, Wolyniec PS, McGrath JA, Steel G, Nestadt G, Liang KY, Huganir RL, et al. (2005). Bipolar I disorder and schizophrenia: a 440-single-nucleotide polymorphism screen of 64 candidate genes among Ashkenazi Jewish case-parent trios. Am. J. Hum. Genet. 77, 918–936. 10.1086/497703. [PubMed: 16380905]
21. Orre M, Kamphuis W, Osborn LM, Jansen AHP, Kooijman L, Bossers K, and Hol EM (2014). Isolation of glia from Alzheimer's mice reveals inflammation and dysfunction. Neurobiol. Aging 35, 2746–2760. 10.1016/j.neurobiolaging.2014.06.004. [PubMed: 25002035]
22. Pereira MSL, Klamt F, Thomé CC, Worm PV, and de Oliveira DL (2017). Metabotropic glutamate receptors as a new therapeutic target for malignant gliomas. Oncotarget 8, 22279–22298. 10.18632/oncotarget.15299. [PubMed: 28212543]
23. Mathys H, Davila-Velderrain J, Peng Z, Gao F, Mohammadi S, Young JZ, Menon M, He L, Abdurrob F, Jiang X, et al. (2019). Single-cell transcriptomic analysis of Alzheimer's disease. Nature 570, 332–337. 10.1038/s41586-019-1195-2. [PubMed: 31042697]
24. Habib N, McCabe C, Medina S, Varshavsky M, Kitsberg D, Dvir-Szternfeld R, Green G, Dionne D, Nguyen L, Marshall JL, et al. (2020). Disease-associated astrocytes in Alzheimer's disease and aging. Nat. Neurosci. 23, 701–706. 10.1038/s41593-020-0624-8. [PubMed: 32341542]
25. Hernandez CM, McQuail JA, Schwabe MR, Burke SN, Setlow B, and Bizon JL (2018). Age-Related Declines in Prefrontal Cortical Expression of Metabotropic Glutamate Receptors that Support Working Memory. eNeuro 5. 10.1523/ENEURO.0164-18.2018.
26. de Quervain DJF, and Papassotiropoulos A (2006). Identification of a genetic cluster influencing memory performance and hippocampal activity in humans. Proc. Natl. Acad. Sci. USA 103, 4270–4274. 10.1073/pnas.0510212103. [PubMed: 16537520]
27. Grubman A, Chew G, Ouyang JF, Sun G, Choo XY, McLean C, Simmons RK, Buckberry S, Vargas-Landin DB, Poppe D, et al. (2019). A single-cell atlas of entorhinal cortex from individuals with Alzheimer's disease reveals cell-type-specific gene expression regulation. Nat. Neurosci. 22, 2087–2097. 10.1038/s41593-019-0539-4. [PubMed: 31768052]
28. Saini SM, Mancuso SG, Mostaid MS, Liu C, Pantelis C, Everall IP, and Bousman CA (2017). Meta-analysis supports GWAS-implicated link between GRM3 and schizophrenia risk. Transl. Psychiatry 7, e1196. 10.1038/tp.2017.172. [PubMed: 28786982]

29. Luessen DJ, and Conn PJ (2022). Allosteric Modulators of Metabotropic Glutamate Receptors as Novel Therapeutics for Neuropsychiatric Disease. Pharmacol. Rev. 74, 630–661. 10.1124/pharmrev.121.000540. [PubMed: 35710132]
30. Li SH, Abd-Elrahman KS, and Ferguson SSG (2022). Targeting mGluR2/3 for treatment of neurodegenerative and neuropsychiatric diseases. Pharmacol. Ther. 239, 108275. 10.1016/j.pharmthera.2022.108275. [PubMed: 36038019]
31. Witkin JM, Pandey KP, and Smith JL (2022). Clinical investigations of compounds targeting metabotropic glutamate receptors. Pharmacol. Biochem. Behav. 219, 173446. 10.1016/j.pbb.2022.173446. [PubMed: 35987339]
32. Deverman BE, Pravdo PL, Simpson BP, Kumar SR, Chan KY, Banerjee A, Wu WL, Yang B, Huber N, Pasca SP, and Gradinaru V (2016). Cre-dependent selection yields AAV variants for widespread gene transfer to the adult brain. Nat. Biotechnol. 34, 204–209. 10.1038/nbt.3440. [PubMed: 26829320]
33. Chan KY, Jang MJ, Yoo BB, Greenbaum A, Ravi N, Wu WL, Sánchez-Guardado L, Lois C, Mazmanian SK, Deverman BE, and Gradinaru V (2017). Engineered AAVs for efficient noninvasive gene delivery to the central and peripheral nervous systems. Nat. Neurosci. 20, 1172–1179. 10.1038/nn.4593. [PubMed: 28671695]
34. Karpf J, Unichenko P, Chalmers N, Beyer F, Wittmann MT, Schneider J, Fidan E, Reis A, Beckervordersandforth J, Brandner S, et al. (2022). Dentate gyrus astrocytes exhibit layer-specific molecular, morphological and physiological features. Nat. Neurosci. 25, 1626–1638. 10.1038/s41593-022-01192-5. [PubMed: 36443610]
35. Lyon L, Kew JNC, Corti C, Harrison PJ, and Burnet PWJ (2008). Altered hippocampal expression of glutamate receptors and transporters in GRM2 and GRM3 knockout mice. Synapse 62, 842–850. 10.1002/syn.20553. [PubMed: 18720515]
36. Vorhees CV, and Williams MT (2006). Morris water maze: procedures for assessing spatial and related forms of learning and memory. Nat. Protoc. 1, 848–858. 10.1038/nprot.2006.116. [PubMed: 17406317]
37. Possin KL, Sanchez PE, Anderson-Bergman C, Fernandez R, Kerchner GA, Johnson ET, Davis A, Lo I, Bott NT, Kiely T, et al. (2016). Cross-species translation of the Morris maze for Alzheimer's disease. J. Clin. Invest. 126, 779–783. 10.1172/JCI78464. [PubMed: 26784542]
38. Maei HR, Zaslavsky K, Teixeira CM, and Frankland PW (2009). What is the Most Sensitive Measure of Water Maze Probe Test Performance? Front. Integr. Neurosci. 3, 4. 10.3389/neuro.07.004.2009. [PubMed: 19404412]
39. Gallagher M, Burwell R, and Burchinal M (1993). Severity of spatial learning impairment in aging: development of a learning index for performance in the Morris water maze. Behav. Neurosci. 107, 618–626. 10.1037//0735-7044.107.4.618. [PubMed: 8397866]
40. Overall RW, Zocher S, Garthe A, and Kempermann G (2020). Rtrack: a software package for reproducible automated water maze analysis. Preprint at bioRxiv, 967372. 10.1101/2020.02.27.967372.
41. Gomez-Ocadiz R, Trippa M, Zhang CL, Posani L, Cocco S, Monasson R, and Schmidt-Hieber C (2022). A synaptic signal for novelty processing in the hippocampus. Nat. Commun. 13, 4122. 10.1038/s41467-022-31775-6. [PubMed: 35840595]
42. Ciocchi S, Passecker J, Malagon-Vina H, Mikus N, and Klausberger T (2015). Brain computation. Selective information routing by ventral hippocampal CA1 projection neurons. Science 348, 560–563. 10.1126/science.aaa3245. [PubMed: 25931556]
43. Hogg S (1996). A review of the validity and variability of the elevated plus-maze as an animal model of anxiety. Pharmacol. Biochem. Behav. 54, 21–30. 10.1016/0091-3057(95)02126-4. [PubMed: 8728535]
44. Walf AA, and Frye CA (2007). The use of the elevated plus maze as an assay of anxiety-related behavior in rodents. Nat. Protoc. 2, 322–328. 10.1038/nprot.2007.44. [PubMed: 17406592]
45. Fujioka R, Nii T, Iwaki A, Shibata A, Ito I, Kitaichi K, Nomura M, Hattori S, Takao K, Miyakawa T, and Fukumaki Y (2014). Comprehensive behavioral study of mGluR3 knockout mice: implication in schizophrenia related endophenotypes. Mol. Brain 7, 31. 10.1186/1756-6606-7-31. [PubMed: 24758191]

46. Markowska AL (1999). Sex dimorphisms in the rate of age-related decline in spatial memory: relevance to alterations in the estrous cycle. J. Neurosci. 19, 8122–8133. 10.1523/JNEUROSCI.19-18-08122.1999. [PubMed: 10479712]
47. Lee Y, Messing A, Su M, and Brenner M (2008). GFAP promoter elements required for region-specific and astrocyte-specific expression. Glia 56, 481–493. 10.1002/glia.20622. [PubMed: 18240313]
48. Tateyama M, Abe H, Nakata H, Saito O, and Kubo Y (2004). Ligand-induced rearrangement of the dimeric metabotropic glutamate receptor 1alpha. Nat. Struct. Mol. Biol. 11, 637–642. 10.1038/nsmb770. [PubMed: 15184890]
49. Lee J, Munguba H, Gutzeit VA, Singh DR, Kristt M, Dittman JS, and Levitz J (2020). Defining the Homo- and Heterodimerization Propensities of Metabotropic Glutamate Receptors. Cell Rep. 31, 107605. 10.1016/j.celrep.2020.107605. [PubMed: 32375054]
50. Berchtold NC, Cribbs DH, Coleman PD, Rogers J, Head E, Kim R, Beach T, Miller C, Troncoso J, Trojanowski JQ, et al. (2008). Gene expression changes in the course of normal brain aging are sexually dimorphic. Proc. Natl. Acad. Sci. USA 105, 15605–15610. 10.1073/pnas.0806883105. [PubMed: 18832152]
51. Yuan Y, Chen YPP, Boyd-Kirkup J, Khaitovich P, and Somel M (2012). Accelerated aging-related transcriptome changes in the female prefrontal cortex. Aging Cell 11, 894–901. 10.1111/j.1474-9726.2012.00859.x. [PubMed: 22783978]
52. Evensmoen HR, Ladstein J, Hansen TI, Møller JA, Witter MP, Nadel L, and Håberg AK (2015). From details to large scale: the representation of environmental positions follows a granularity gradient along the human hippocampal and entorhinal anterior-posterior axis. Hippocampus 25, 119–135. 10.1002/hipo.22357. [PubMed: 25155295]
53. Epstein RA, Patai EZ, Julian JB, and Spiers HJ (2017). The cognitive map in humans: spatial navigation and beyond. Nat. Neurosci. 20, 1504–1513. 10.1038/nn.4656. [PubMed: 29073650]
54. Evensmoen HR, Rimol LM, Winkler AM, Betzel R, Hansen TI, Nili H, and Håberg A (2021). Allocentric representation in the human amygdala and ventral visual stream. Cell Rep. 34, 108658. 10.1016/j.celrep.2020.108658. [PubMed: 33472067]
55. Orr AG, Lo I, Schumacher H, Ho K, Gill M, Guo W, Kim DH, Knox A, Saito T, Saido TC, et al. (2018). Istradefylline reduces memory deficits in aging mice with amyloid pathology. Neurobiol. Dis. 110, 29–36. 10.1016/j.nbd.2017.10.014. [PubMed: 29100987]
56. Armbruster BN, Li X, Pausch MH, Herlitze S, and Roth BL (2007). Evolving the lock to fit the key to create a family of G protein-coupled receptors potently activated by an inert ligand. Proc. Natl. Acad. Sci. USA 104, 5163–5168. 10.1073/pnas.0700293104. [PubMed: 17360345]
57. Chai H, Diaz-Castro B, Shigetomi E, Monte E, Octeau JC, Yu X, Cohn W, Rajendran PS, Vondriska TM, Whitelegge JP, et al. (2017). Neural Circuit-Specialized Astrocytes: Transcriptomic, Proteomic, Morphological, and Functional Evidence. Neuron 95, 531–549.e9. 10.1016/j.neuron.2017.06.029. [PubMed: 28712653]
58. Li D, Hérault K, Zylbersztejn K, Lauterbach MA, Guillon M, Oheim M, and Ropert N (2015). Astrocyte VAMP3 vesicles undergo Ca2+ -independent cycling and modulate glutamate transporter trafficking. J. Physiol. 593, 2807–2832. 10.1113/JP270362. [PubMed: 25864578]
59. Durand D, Carniglia L, Caruso C, and Lasaga M (2011). Reduced cAMP, Akt activation and p65-c-Rel dimerization: mechanisms involved in the protective effects of mGluR3 agonists in cultured astrocytes. PLoS One 6, e22235. 10.1371/journal.pone.0022235. [PubMed: 21779400]
60. Gomez JL, Bonaventura J, Lesniak W, Mathews WB, Sysa-Shah P, Rodriguez LA, Ellis RJ, Richie CT, Harvey BK, Dannals RF, et al. (2017). Chemogenetics revealed: DREADD occupancy and activation via converted clozapine. Science 357, 503–507. 10.1126/science.aan2475. [PubMed: 28774929]
61. Kofuji P, and Araque A (2021). G-Protein-Coupled Receptors in Astrocyte-Neuron Communication. Neuroscience 456, 71–84. 10.1016/j.neuroscience.2020.03.025. [PubMed: 32224231]
62. McGraw DW, Elwing JM, Fogel KM, Wang WCH, Glinka CB, Mihlbachler KA, Rothenberg ME, and Liggett SB (2007). Crosstalk between Gi and Gq/Gs pathways in airway smooth

muscle regulates bronchial contractility and relaxation. J. Clin. Invest. 117, 1391–1398. 10.1172/JCI30489. [PubMed: 17415415]

63. Kofalvi A, Moreno E, Cordomi A, Cai NS, Fernandez-Duenas V, Ferreira SG, Guixa-Gonzalez R, Sanchez-Soto M, Yano H, Casado-Anguera V, et al. (2020). Control of glutamate release by complexes of adenosine and cannabinoid receptors. BMC Biol. 18, 9. 10.1186/s12915-020-0739-0. [PubMed: 31973708]
64. Guettier JM, Gautam D, Scarselli M, Ruiz de Azua I, Li JH, Rosemond E, Ma X, Gonzalez FJ, Armbruster BN, Lu H, et al. (2009). A chemical-genetic approach to study G protein regulation of beta cell function in vivo. Proc. Natl. Acad. Sci. USA 106, 19197–19202. 10.1073/pnas.0906593106. [PubMed: 19858481]
65. Zhou Z, Okamoto K, Onodera J, Hiragi T, Andoh M, Ikawa M, Tanaka KF, Ikegaya Y, and Koyama R (2021). Astrocytic cAMP modulates memory via synaptic plasticity. Proc. Natl. Acad. Sci. USA 118, e2016584118. 10.1073/pnas.2016584118. [PubMed: 33452135]
66. Runegaard AH, Fitzpatrick CM, Woldbye DPD, Andreasen JT, Sørensen AT, and Gether U (2019). Modulating Dopamine Signaling and Behavior with Chemogenetics: Concepts, Progress, and Challenges. Pharmacol. Rev. 71, 123–156. 10.1124/pr.117.013995. [PubMed: 30814274]
67. Yagi S, and Galea LAM (2019). Sex differences in hippocampal cognition and neurogenesis. Neuropsychopharmacology 44, 200–213. 10.1038/s41386-018-0208-4. [PubMed: 30214058]
68. Velasco ER, Florido A, Milad MR, and Andero R (2019). Sex differences in fear extinction. Neurosci. Biobehav. Rev. 103, 81–108. 10.1016/j.neubiorev.2019.05.020. [PubMed: 31129235]
69. Jain A, Huang GZ, and Woolley CS (2019). Latent Sex Differences in Molecular Signaling That Underlies Excitatory Synaptic Potentiation in the Hippocampus. J. Neurosci. 39, 1552–1565. 10.1523/JNEUROSCI.1897-18.2018. [PubMed: 30578341]
70. McEwen BS, and Milner TA (2017). Understanding the broad influence of sex hormones and sex differences in the brain. J. Neurosci. Res. 95, 24–39. 10.1002/jnr.23809. [PubMed: 27870427]
71. Galea LAM, Choleris E, Albert AYK, McCarthy MM, and Sohrabji F (2020). The promises and pitfalls of sex difference research. Front. Neuroendocrinol. 56, 100817. 10.1016/j.yfrne.2019.100817. [PubMed: 31837339]
72. Shansky RM, and Woolley CS (2016). Considering Sex as a Biological Variable Will Be Valuable for Neuroscience Research. J. Neurosci. 36, 11817–11822. 10.1523/JNEUROSCI.1390-16.2016. [PubMed: 27881768]
73. McCarthy MM, Woolley CS, and Arnold AP (2017). Incorporating sex as a biological variable in neuroscience: what do we gain? Nat. Rev. Neurosci. 18, 707–708. 10.1038/nrn.2017.137. [PubMed: 29097784]
74. Yu X, Nagai J, Marti-Solano M, Soto JS, Coppola G, Babu MM, and Khakh BS (2020). Context-Specific Striatal Astrocyte Molecular Responses Are Phenotypically Exploitable. Neuron 108, 1146–1162.e10. 10.1016/j.neuron.2020.09.021. [PubMed: 33086039]
75. MacDonald AJ, Holmes FE, Beall C, Pickering AE, and Ellacott KLJ (2020). Regulation of food intake by astrocytes in the brainstem dorsal vagal complex. Glia 68, 1241–1254. 10.1002/glia.23774. [PubMed: 31880353]
76. Mederos S, Sánchez-Puelles C, Esparza J, Valero M, Ponomarenko A, and Perea G (2021). GABAergic signaling to astrocytes in the prefrontal cortex sustains goal-directed behaviors. Nat. Neurosci. 24, 82–92. 10.1038/s41593-020-00752-x. [PubMed: 33288910]
77. Rurak GM, Simard S, Freitas-Andrade M, Lacoste B, Charih F, Van Geel A, Stead J, Woodside B, Green JR, Coppola G, and Salmaso N (2022). Sex differences in developmental patterns of neocortical astroglia: A mouse translatome database. Cell Rep. 38, 110310. 10.1016/j.celrep.2022.110310. [PubMed: 35108542]
78. Gonzalez-Vila A, Luengo-Mateos M, Silveira-Loureiro M, Garrido-Gil P, Ohinska N, Gonzalez-Dominguez M, Labandeira-Garcia JL, Garcia-Caceres C, Lopez M, and Barca-Mayo O (2023). Astrocytic insulin receptor controls circadian behavior via dopamine signaling in a sexually dimorphic manner. Nat. Commun. 14, 8175. 10.1038/s41467-023-44039-8. [PubMed: 38071352]
79. Dong C, Madar AD, and Sheffield MEJ (2021). Distinct place cell dynamics in CA1 and CA3 encode experience in new environments. Nat. Commun. 12, 2977. 10.1038/s41467-021-23260-3. [PubMed: 34016996]

80. Goode LK, Fusilier AR, Remiszewski N, Reeves JM, Abiraman K, Defenderfer M, Paul JR, McMahon LL, and Gamble KL (2022). Examination of Diurnal Variation and Sex Differences in Hippocampal Neurophysiology and Spatial Memory. eNeuro 9. 10.1523/ENEURO.0124-22.2022.
81. Wilson IA, Ikonen S, Gallagher M, Eichenbaum H, and Tanila H (2005). Age-associated alterations of hippocampal place cells are subregion specific. J. Neurosci. 25, 6877–6886. 10.1523/JNEUROSCI.1744-05.2005. [PubMed: 16033897]
82. Wilson IA, Gallagher M, Eichenbaum H, and Tanila H (2006). Neurocognitive aging: prior memories hinder new hippocampal encoding. Trends Neurosci. 29, 662–670. 10.1016/j.tins.2006.10.002. [PubMed: 17046075]
83. Haberman RP, Koh MT, and Gallagher M (2017). Heightened cortical excitability in aged rodents with memory impairment. Neurobiol. Aging 54, 144–151. 10.1016/j.neurobiolaging.2016.12.021. [PubMed: 28104309]
84. Yassa MA, Lacy JW, Stark SM, Albert MS, Gallagher M, and Stark CEL (2011). Pattern separation deficits associated with increased hippocampal CA3 and dentate gyrus activity in nondemented older adults. Hippocampus 21, 968–979. 10.1002/hipo.20808. [PubMed: 20865732]
85. Robitsek J, Ratner MH, Stewart T, Eichenbaum H, and Farb DH (2015). Combined administration of levetiracetam and valproic acid attenuates age-related hyperactivity of CA3 place cells, reduces place field area, and increases spatial information content in aged rat hippocampus. Hippocampus 25, 1541–1555. 10.1002/hipo.22474. [PubMed: 25941121]
86. Benice TS, Rizk A, Kohama S, Pfankuch T, and Raber J (2006). Sex-differences in age-related cognitive decline in C57BL/6J mice associated with increased brain microtubule-associated protein 2 and synaptophysin immunoreactivity. Neuroscience 137, 413–423. 10.1016/j.neuroscience.2005.08.029. [PubMed: 16330151]
87. LaChance PA, Todd TP, and Taube JS (2019). A sense of space in postrhinal cortex. Science 365, eaax4192. 10.1126/science.aax4192. [PubMed: 31296737]
88. Alexander AS, Robinson JC, Stern CE, and Hasselmo ME (2023). Gated transformations from egocentric to allocentric reference frames involving retrosplenial cortex, entorhinal cortex, and hippocampus. Hippocampus 33, 465–487. 10.1002/hipo.23513. [PubMed: 36861201]
89. van Wijngaarden JB, Babl SS, and Ito HT (2020). Entorhinal-retrosplenial circuits for allocentric-egocentric transformation of boundary coding. Elife 9, e59816. 10.7554/eLife.59816. [PubMed: 33138915]
90. Koss WA, Haertel JM, Philippi SM, and Frick KM (2018). Sex Differences in the Rapid Cell Signaling Mechanisms Underlying the Memory-Enhancing Effects of 17beta-Estradiol. eNeuro 5. 10.1523/ENEURO.0267-18.2018.
91. Lazennec G, Thomas JA, and Katzenellenbogen BS (2001). Involvement of cyclic AMP response element binding protein (CREB) and estrogen receptor phosphorylation in the synergistic activation of the estrogen receptor by estradiol and protein kinase activators. J. Steroid Biochem. Mol. Biol. 77, 193–203. 10.1016/s0960-0760(01)00060-7. [PubMed: 11457657]
92. Bracchi-Ricard V, Brambilla R, Levenson J, Hu WH, Bramwell A, Sweatt JD, Green EJ, and Bethea JR (2008). Astroglial nuclear factor-kappaB regulates learning and memory and synaptic plasticity in female mice. J. Neurochem. 104, 611–623. 10.1111/j.1471-4159.2007.04993.x. [PubMed: 17953667]
93. Baier MP, Nagaraja RY, Yarbrough HP, Owen DB, Masingale AM, Ranjit R, Stiles MA, Murphy A, Agbaga MP, Ahmad M, et al. (2022). Selective ablation of Sod2 in astrocytes induces sex-specific effects on cognitive function, D-serine availability, and astrogliosis. J. Neurosci. 42, 5992–6006. 10.1523/JNEUROSCI.2543-21.2022. [PubMed: 35760531]
94. Hamson DK, Roes MM, and Galea LAM (2016). Sex Hormones and Cognition: Neuroendocrine Influences on Memory and Learning. Compr. Physiol. 6, 1295–1337. 10.1002/cphy.c150031. [PubMed: 27347894]
95. Torromino G, Loffredo V, Cavezza D, Sonsini G, Esposito F, Crevenna AH, Gioffrè M, De Risi M, Treves A, Griguoli M, and De Leonibus E (2022). Thalamo-hippocampal pathway regulates incidental memory capacity in mice. Nat. Commun. 13, 4194. 10.1038/s41467-022-31781-8. [PubMed: 35859057]

96. Sprissler RS, Wagnon JL, Bunton-Stasyshyn RK, Meisler MH, and Hammer MF (2017). Altered gene expression profile in a mouse model of SCN8A encephalopathy. Exp. Neurol. 288, 134–141. 10.1016/j.expneurol.2016.11.002. [PubMed: 27836728]

97. Velmeshev D, Schirmer L, Jung D, Haeussler M, Perez Y, Mayer S, Bhaduri A, Goyal N, Rowitch DH, and Kriegstein AR (2019). Single-cell genomics identifies cell type-specific molecular changes in autism. Science 364, 685–689. 10.1126/science.aav8130. [PubMed: 31097668]

98. Diaz-Castro B, Gangwani MR, Yu X, Coppola G, and Khakh BS (2019). Astrocyte molecular signatures in Huntington's disease. Sci. Transl. Med. 11, eaaw8546. 10.1126/scitranslmed.aaw8546. [PubMed: 31619545]

99. Ferretti MT, Iulita MF, Cavedo E, Chiesa PA, Schumacher Dimech A, Santuccione Chadha A, Baracchi F, Girouard H, Misoch S, Giacobini E, et al. (2018). Sex differences in Alzheimer disease — the gateway to precision medicine. Nat. Rev. Neurol. 14, 457–469. 10.1038/s41582-018-0032-9. [PubMed: 29985474]

100. Zimmer TS, Orr AL, and Orr AG (2024). Astrocytes in selective vulnerability to neurodegenerative disease. Trends Neurosci. 47, 289–302. 10.1016/j.tins.2024.02.008. [PubMed: 38521710]

101. Lee BH, Richard JE, de Leon RG, Yagi S, and Galea LAM (2023). Sex Differences in Cognition Across Aging. Curr. Top. Behav. Neurosci. 62, 235–284. 10.1007/7854_2022_309. [PubMed: 35467294]

102. Pallier PN, Ferrara M, Romagnolo F, Ferretti MT, Soreq H, and Cerase A (2022). Chromosomal and environmental contributions to sex differences in the vulnerability to neurological and neuropsychiatric disorders: Implications for therapeutic interventions. Prog. Neurobiol. 219, 102353. 10.1016/j.pneurobio.2022.102353. [PubMed: 36100191]

103. Hung SSC, Chrysostomou V, Li F, Lim JKH, Wang JH, Powell JE, Tu L, Daniszewski M, Lo C, Wong RC, et al. (2016). AAV-Mediated CRISPR/Cas Gene Editing of Retinal Cells In Vivo. Invest. Ophthalmol. Vis. Sci. 57, 3470–3476. 10.1167/iovs.16-19316. [PubMed: 27367513]

104. Wilusz JE, JnBaptiste CK, Lu LY, Kuhn CD, Joshua-Tor L, and Sharp PA (2012). A triple helix stabilizes the 3' ends of long noncoding RNAs that lack poly(A) tails. Genes Dev. 26, 2392–2407. 10.1101/gad.204438.112. [PubMed: 23073843]

105. Rotheneichner P, Romanelli P, Bieler L, Pagitsch S, Zaunmair P, Kreutzer C, Kö nig R, Marschallinger J, Aigner L, and CouillardDespré s S (2017). Tamoxifen Activation of Cre-Recombinase Has No Persisting Effects on Adult Neurogenesis or Learning and Anxiety. Front. Neurosci. 11, 27. 10.3389/fnins.2017.00027. [PubMed: 28203140]

106. Valny M, Honsa P, Kirdajova D, Kamenik Z, and Anderova M (2016). Tamoxifen in the Mouse Brain: Implications for Fate-Mapping Studies Using the Tamoxifen-Inducible Cre-loxP System. Front. Cell. Neurosci. 10, 243. 10.3389/fncel.2016.00243. [PubMed: 27812322]

107. Labun K, Montague TG, Gagnon JA, Thyme SB, and Valen E (2016). CHOPCHOP v2: a web tool for the next generation of CRISPR genome engineering. Nucleic Acids Res. 44, W272–W276. 10.1093/nar/gkw398. [PubMed: 27185894]

108. Diamond DM, Campbell AM, Park CR, Woodson JC, Conrad CD, Bachstetter AD, and Mervis RF (2006). Influence of predator stress on the consolidation versus retrieval of long-term spatial memory and hippocampal spinogenesis. Hippocampus 16, 571–576. 10.1002/hipo.20188. [PubMed: 16741974]

109. Kim JJ, Koo JW, Lee HJ, and Han JS (2005). Amygdalar inactivation blocks stress-induced impairments in hippocampal long-term potentiation and spatial memory. J. Neurosci. 25, 1532–1539. 10.1523/JNEUROSCI.4623-04.2005. [PubMed: 15703407]

110. Holscher C (1999). Stress impairs performance in spatial water maze learning tasks. Behav. Brain Res. 100, 225–235. 10.1016/s0166-4328(98)00134-x. [PubMed: 10212070]

111. Garthe A, Behr J, and Kempermann G (2009). Adult-generated hippocampal neurons allow the flexible use of spatially precise learning strategies. PLoS One 4, e5464. 10.1371/journal.pone.0005464. [PubMed: 19421325]

Highlights

- Changes in astrocytic mGluR3 levels induce sex-dependent effects on spatial memory
- Astrocytic mGluR3 modulates search behavior at recall in a sex-specific manner
- Astrocytic $G_{i/o}$ and G_s receptors have opposing, sex-dimorphic effects on memory

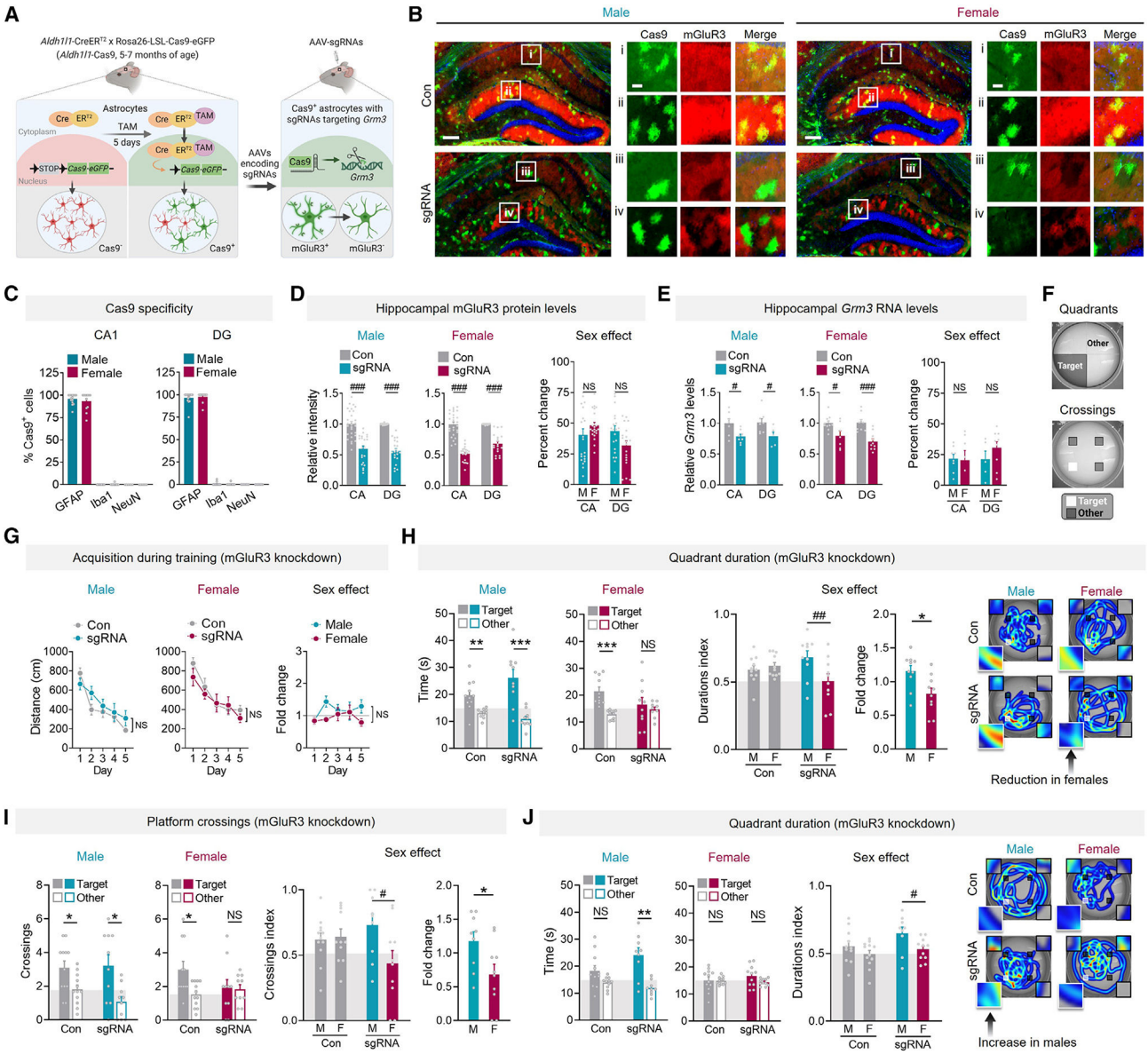

Figure 1. Reductions in astrocytic mGluR3 levels cause sex-specific effects on memory

(A) Schematic of astrocytic *Grm3* knockdown.

(B) Cas9-EGFP (green) and mGluR3 (red) in hippocampus of *Aldh1l1*-Cas9 mice (5–7 months of age) injected with vehicle (Con) or AAVs encoding sgRNAs. DAPI (blue) labeled cell nuclei. Scale bars: 400 μm and 80 μm (insets).

(C) Analyses of Cas9-EGFP-positive cell types: astrocytes (GFAP), microglia/macrophages (Iba1), neurons (NeuN) in the cornu Ammonis (CA) and dentate gyrus (DG). $n = 6–17$ mice/sex/labeling condition.

(D) mGluR3 in the CA and DG. Data were normalized per sex and region. See Figure S1F for endogenous mGluR3. Two-way ANOVA (males): $F(1, 99) = 138.8$, $p < 0.001$; (females): $F(1, 90) = 194.0$, $p < 0.001$ for main effect of knockdown. Sidak's test (vs. control (Con) or other sex, as indicated): $^{###}p < 0.001$. $n = 5–6$ mice/sex/condition.

(E) Hippocampal *Grm3* mRNA levels. Data were normalized per sex and region. Two-way ANOVA (males): $F(1, 24) = 12.61$, $p = 0.0016$; (females): $F(1, 33) = 26.52$, $p < 0.001$ for main effect of knockdown. Sidak's test (vs. Con or other sex): $^{\#}p < 0.05$ and $^{\#\#\#}p < 0.001$. $n = 5–11$ mice/sex/region/condition.

(F) Target and other arena areas assessed for cumulative quadrant durations and platform location crossings.

(G) Mean distance traveled during training in the Morris water maze.

(H and I) Target quadrant durations (H) and platform crossings (I) compared to other locations in probe 1 day after training. Two-way ANOVA (durations index): $F(1, 38) = 6.42$, $p = 0.016$; (crossings index): $F(1, 38) = 4.56$, $p = 0.039$ for interaction effect. Sidak's test: $^{\#}p < 0.05$ and $^{\#\#}p < 0.01$.

(J) Target quadrant durations in probe 9 days after training. Two-way ANOVA (durations index): $F(1, 39) = 6.90$, $p = 0.012$ for sex effect. Sidak's test: $^{\#}p < 0.05$. Heatmaps in (H) and (J) show representative swim paths; target and other locations are highlighted (insets). Student's t test: $^{*}p < 0.05$, $^{**}p < 0.01$, and $^{***}p < 0.001$. $n = 10–12$ mice/sex/condition (G–J). NS, no significant preference. Data are mean ± SEM.

See also Figures S1 and S2, and Table S2.

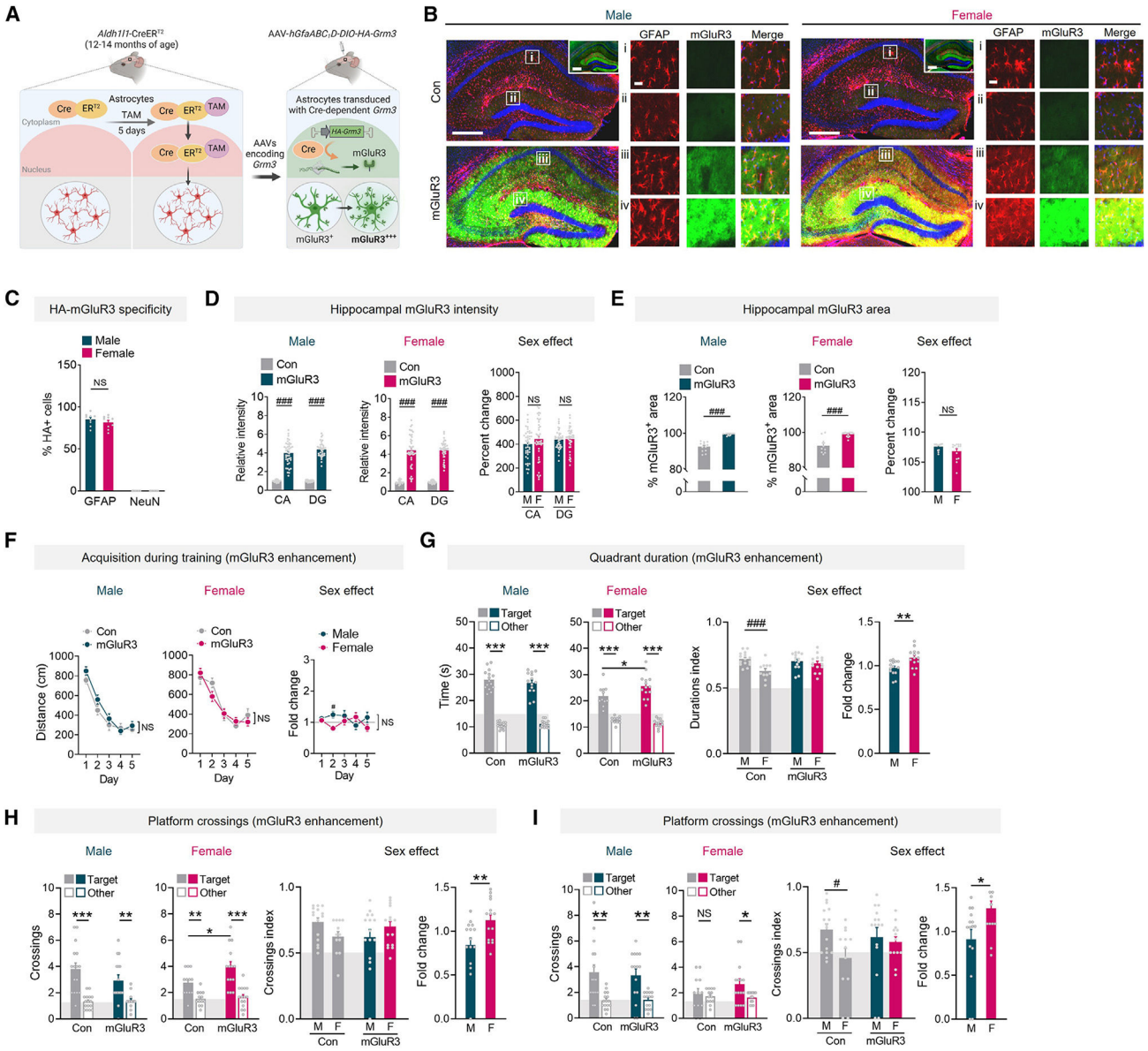

Figure 2. Astrocytic mGluR3 enhancement improves memory in females but not males

(A) Schematic of the two-promoter system for enhancing mGluR3.

(B) GFAP (red) and mGluR3 (green) in hippocampus of *Aldh1l1*-CreER^{T2} mice (12–14 months of age) injected with vehicle (Con) or AAVs encoding mGluR3. DAPI (blue) labeled cell nuclei. Scale bars: 400 μm and 40 μm (insets i–iv). Inlays show the same sections at longer exposure.

(C) GFAP-positive and NeuN-positive cells in the DG that were also HA positive. Two-way ANOVA: $F(1, 32) = 2242$, $p < 0.001$ for main effect of cell marker; $F(1, 32) = 1.057$, $p = 0.311$ for main effect of sex; $F(1, 39) = 16.66$, $p = 0.0002$ for interaction. $n = 9$ mice per sex.

(D) mGluR3 immunofluorescence in the CA and DG. Two-way ANOVA (males): $F(1, 141) = 622.4$, $p < 0.001$; (females): $F(1, 141) = 368.3$, $p < 0.001$ for main effect of mGluR3 enhancement. Sidak's test (vs. Con or other sex): $^{###}p < 0.001$. $n = 11–15$ mice/sex/condition.

(E) mGluR3 immunolabeling in DG. Two-way ANOVA: $F(1, 45) = 86.50$, $^{###}p < 0.001$ for main effect. Sidak's test (vs. Con): $^{###}p < 0.001$. $n = 10–14$ mice/sex/condition.
(F) Mean distance traveled during training in the Morris water maze.
(G and H) Target quadrant durations (G) and platform crossings (H) in probe 1 day after training. Two-way ANOVA (durations index): $F(1, 50) = 5.33$, $p = 0.025$; (crossings index): $F(1, 53) = 4.68$, $p = 0.035$ for interaction effects. Sidak's test: $^{#}p < 0.05$ and $^{##}p < 0.01$.
(I) Target crossings in probe 9 days after training. Two-way ANOVA (crossings index): $F(1, 52) = 4.36$, $p = 0.04$ for sex effect. Sidak's test: $^{#}p < 0.05$. Student's t test: $*p < 0.05$, $**p < 0.01$, and $***p < 0.001$. $n = 12–16$ mice/sex/condition (F–I). NS, no significant preference. Data are mean ± SEM.
See also Figures S3–S5 and Table S2.

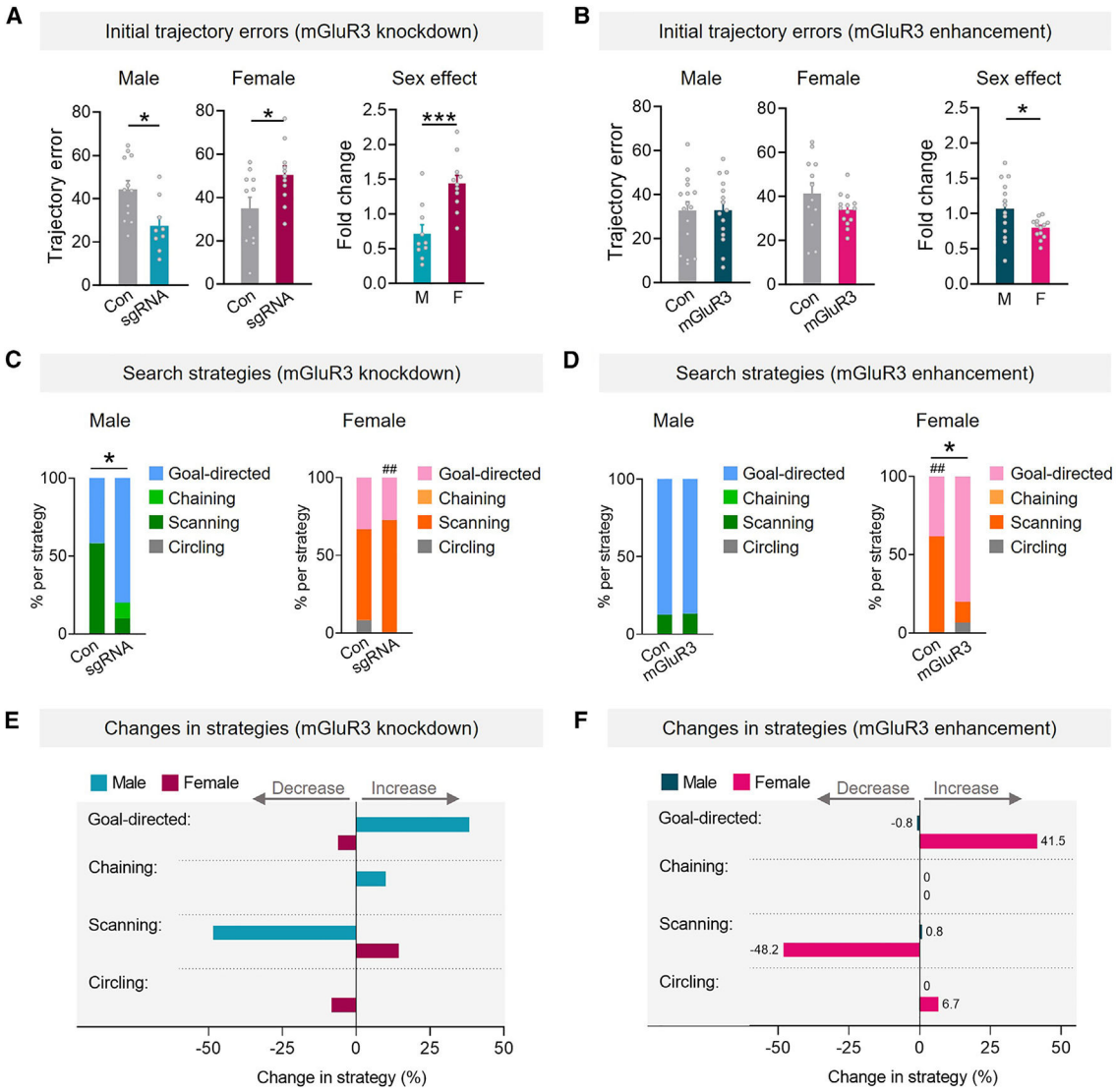

Figure 3. Changes in astrocytic mGluR3 regulate search behavior in a sex-specific manner

(A and B) Initial trajectory errors during probe 9 days after training in mice with reduced (A) or increased (B) mGluR3. Student's t test: *$p < 0.05$ and ***$p < 0.001$.

(C and D) Frequency of different search strategies. Control males showed higher goal-directed strategies in (D), possibly due to differences between transgenic lines and other factors. Fisher's exact test, one sided: *$p < 0.05$ vs. Con; $^{\#\#}p < 0.01$ vs. males.

(E and F) Changes in the frequency of strategies.

n = 10–12 (A, C, and E) and 12–16 (B, D, and F) mice/sex/condition. Data are mean ± SEM (A and B) or percentiles (C–F).

See also Figure S6 and Table S2.

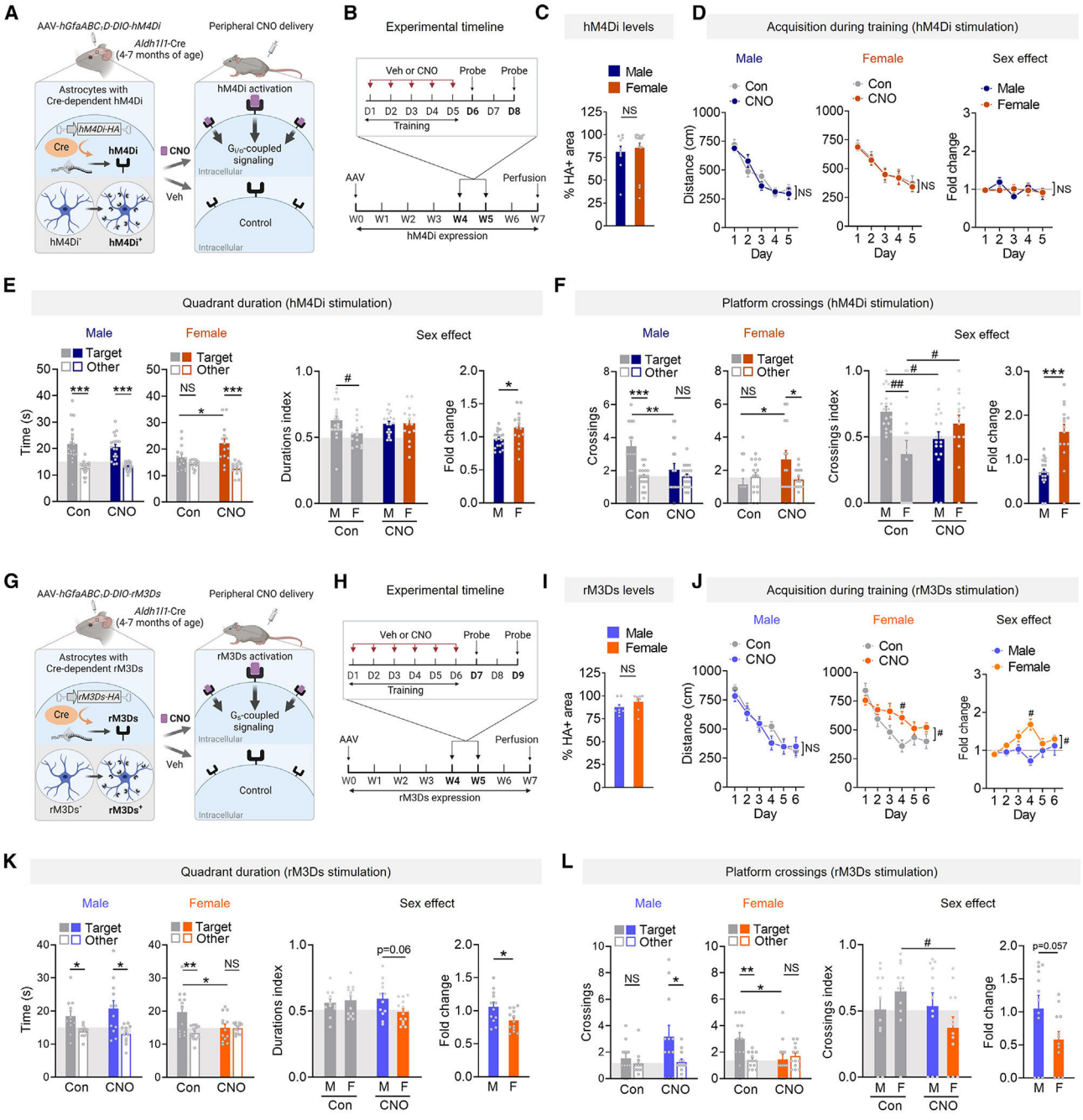

Figure 4. Stimulation of astrocytic G-protein-coupled signaling has bidirectional, sex-dimorphic effects on memory

(A) Schematic of inducible expression and activation of hM4Di.

(B) Timeline for hM4Di-expressing mice.

(C) HA-positive area in the dentate gyrus molecular layer. n = 10–17 mice per sex.

(D) Mean distance traveled by 4- to 7-month-old hM4Di-expressing mice during training. Three-way ANOVA: $F(4, 288) = 0.000$, $p > 0.999$ for interaction effect.

(E and F) Probe 3 days after training. Target quadrant durations (E) and platform crossings (F). Two-way ANOVA (durations index): $F(1, 62) = 3.18$, $p = 0.079$ for interaction; (crossings index): $F(1, 62) = 11.46$, $p = 0.0012$ for interaction.

(G) Schematic of inducible expression and activation of rM3Ds.

(H) Timeline for rM3Ds-expressing mice.

(I) HA-positive area in the DGmol. $n = 8$ mice per sex.

(J) Mean distance traveled by 4- to 7-month-old rM3Ds-expressing mice during training. Three-way ANOVA: $F(5, 210) = 0.000$, $p > 0.999$ for interaction effect. Two-way ANOVA: $F(5, 120) = 2.39$, $p = 0.042$ for interaction effect in females (time, CNO); $F(5, 115) = 4.69$, $p = 0.0006$ for sex effect. Sidak's test: $^{\#}p < 0.05$.

(K and L) Probe 3 days after training. Target quadrant durations (K) and platform crossings (L). Two-way ANOVA (durations index): $F(1, 45) = 3.53$, $p = 0.067$ for interaction; (crossings index): $F(1, 41) = 3.82$, $p = 0.057$ for interaction. Sidak's test: $^{\#}p < 0.05$ and $^{\#\#}p < 0.01$.

Student's t test: $^{*}p < 0.05$, $^{**}p < 0.01$, and $^{***}p < 0.001$. $n = 15$–19 mice/sex/condition (D–F). $n = 12$–13 mice/sex/condition (J–L). NS, no significant preference. Data are mean ± SEM.

See also Figures S7–S9 and Table S2.

KEY RESOURCES TABLE

REAGENT or RESOURCE	SOURCE	IDENTIFIER
Antibodies		
Mouse anti-HA	Biolegend	Cat # 901513; RRID: AB_2565335
Rabbit anti-HA	Cell Signaling	Cat # 3724S; RRID: AB_1549585
Rabbit anti-GFAP	MilliporeSigma	Cat # G9269; RRID: AB_477035
Mouse anti-GFAP	MilliporeSigma	Cat # MAB3402B; RRID: AB_10917109
Goat anti-GFAP	Abcam	Cat # ab53554; RRID: AB_880202
Chicken anti-GFAP	Abcam	Cat # ab4674; RRID: AB_304558
Rabbit anti-mGluR3	Abcam	Cat # ab166608; RRID: AB_2833092
Chicken anti-GFP	Abcam	Cat # ab13970; RRID: AB_300798
Rabbit anti-NeuN	MilliporeSigma	Cat # ABN78; RRID: AB_10807945
Guinea pig anti-NeuN	MilliporeSigma	Cat # ABN90; RRID: AB_11205592
Goat anti-Iba1	Abcam	Cat # ab5076; RRID: AB_222402
Rabbit anti-phospho-CREB (S133)	Cell Signaling	Cat # 9198; RRID: AB_2561044
Mouse anti-total-CREB	Cell Signaling	Cat # 9104S; RRID: AB_490881
Rabbit anti-phospho-Akt (Ser473)	Abcam	Cat # ab81283; RRID: AB_2224551
Mouse anti-total-Akt	Cell Signaling	Cat # 2920S; RRID: AB_1147620
Mouse anti-γ-tubulin	MilliporeSigma	Cat # T5326; RRID: AB_532292
Mouse anti-*c*-Fos	Abcam	Cat # ab208942; RRID: AB_2747772
Bacterial and viral strains		
AAV2/PHP.eB-*U6*-sgRNA552	In paper	N/A
AAV2/PHP.eB-*U6*-sgRNA703	In paper	N/A
AAV2/PHP.eB-*hGfaABC1D*-DIO-HA-mGluR3	In paper	N/A
AAV2/PHP.eB-*hGfaABC1D*-DIO-HA-hM4Di	In paper	N/A
AAV2/PHP.eB-*hGfaABC1D*-DIO-HA-rM3Ds	In paper	N/A
Chemicals, peptides, and recombinant proteins		
Clozapine-N-oxide	Tocris	Cat # 4936
LY354740	Tocris	Cat # 3246
2,2,2-tribromoethanol	Fisher Scientific	Cat # AC421430100
4',6-Diamidino-2-phenylindole dihydrochloride (DAPI)	MilliporeSigma	Cat # D9542
Tamoxifen (TAM)	MilliporeSigma	Cat # T5648
Critical commercial assays		
Platinum SuperFi DNA Polymerase kit	ThermoFisher	Cat #12351010
Plasmid Plus Maxi Prep kit	Qiagen	Cat # 12963
RNeasy Mini Kit with DNase	Qiagen	Cat # 74106; #79256
Protoscript First Strand Synthesis Kit	New England Biolabs	Cat # 6300L

REAGENT or RESOURCE	SOURCE	IDENTIFIER
Experimental models: Cell lines		
NEB 5-alpha competent bacteria	New England Biolabs	Cat # C2987H
Experimental models: Organisms/strains		
Aldh1l1-CreER^{T2} mice (12–14 months of age)	Jackson Laboratory	Strain 031008
Rosa26-LSL-Cas9 mice (used in crossing lines; up to 12 months of age)	Jackson Laboratory	Strain 026556
Aldh1l1-Cre mice (4–7 months of age)	Jackson Laboratory	Strain 023748
Aldh1l1-CreER^{T2} x Rosa26-LSL-Cas9 *(Aldh1l1-Cas9)* mice; 5–7 months of age)	This paper	N/A
Wild-type C57BL/6J mice (up to 12 months of age)	Jackson Laboratory	Strain 000664
Oligonucleotides		
#552 forward, CACCGCAGAGGTATCCAACGCCTGG	This paper	N/A
#552 reverse, AAACCCAGGCGTTGGATACCTCTGC	This paper	N/A
#703 forward, CCGCAGAGCATCGTTGACTAAAG	This paper	N/A
#703 reverse, AACCTTTAGTCAACGATGCTCTGC	This paper	N/A
See Table S4 for RT-qPCR primer sequences	This paper	N/A
Recombinant DNA		
pAAV-*U6*-sgRNA-hSyn-mCherry vector	Addgene; Hung et al.[103]	Addgene #87916; RRID: Addgene 87916
pAAV-*GFAP*-EGFP	Addgene	Addgene #50473; RRID: Addgene_50473
pAAV-*EF1a*-DIO-hM4D(Gi)-mCherry	Addgene	Addgene #50461; RRID: Addgene_50461
pCRII-TOPO *CMV*-cGFP-bGH Poly(A)	Addgene; Wilusz et al.[104]	Addgene #46835; RRID: Addgene_46835
pAAV-*GFAP*-HA-hM4D(Gi)-IRES-mCitrine	Addgene	Addgene #50471; RRID: Addgene_50471
pAAV-*GFAP*-HA-rM3D(Gs)-IRES-mCitrine	Addgene	Addgene #50472; RRID: Addgene_50472
Software and algorithms		
Ethovision XT (version 12.0.1138)	Noldus	N/A
R Studio (version 4.0.3)		N/A
Rtrack package (version 1.0.0)	Overall et al.[40]	https://rupertoverall.net/Rtrack/
GraphPad Prism (version 8 or above)		N/A
BZ-X Analyzer Software	Keyence	N/A
ImageJ (FIJI)		N/A